JAERI-M
87-046

ANNUAL REPORT OF THE OSAKA LABORATORY FOR RADIATION CHEMISTRY JAPAN ATOMIC ENERGY RESEARCH INSTITUTE

(No. 19)

April, 1985—March 31, 1986

March 1987

Osaka Laboratory Radiation Chemistry

日 本 原 子 力 研 究 所
Japan Atomic Energy Research Institute

JAERI-Mレポートは，日本原子力研究所が不定期に公刊している研究報告書です。
入手の問合わせは，日本原子力研究所技術情報部情報資料課（〒319－11茨城県那珂郡東海村）あて，お申しこしください。なお，このほかに財団法人原子力弘済会資料センター（〒319-11茨城県那珂郡東海村日本原子力研究所内）で複写による実費頒布をおこなっております。

JAERI-M reports are issued irregularly.
Inquiries about availability of the reports should be addressed to Information Division, Department of Technical Information, Japan Atomic Energy Research Institute, Tokai-mura, Naka-gun, Ibaraki-ken 319-11, Japan.

編集兼発行　日本原子力研究所
印　　刷　日立高速印刷株式会社

JAERI-M 87-046

ANNUAL REPORT OF THE OSAKA LABORATORY FOR RADIATION CHEMISTRY JAPAN ATOMIC ENERGY RESEARCH INSTITUTE

(No. 19)
April 1, 1985 - March 31, 1986

Osaka Laboratory for Radiation Chemistry
Takasaki Radiation Chemistry Research Establishment
Japan Atomic Energy Research Institute
Neyagawa-shi, Osaka 572 JAPAN
(Received February 18, 1987)

This report describes research activities of Osaka Laboratory for Radiation Chemistry, JAERI during one year period from April 1, 1985 through March 31, 1986. The latest report, for 1984, is JAERI-M 86-051.

Detailed descriptions of the activities are presented in the following subjects: studies on surface phenomena under electron and ion irradiations; polymerization under the irradiation of electron beams; modification of polymers, degradation, cross-linking, and grafting.

Previous reports in this series are:

Annual Report, JARRP, Vol. 1		1958/1959*
Annual Report, JARRP, Vol. 2		1960
Annual Report, JARRP, Vol. 3		1961
Annual Report, JARRP, Vol. 4		1962
Annual Report, JARRP, Vol. 5		1963
Annual Report, JARRP, Vol. 6		1964
Annual Report, JARRP, Vol. 7		1965
Annual Report, JARRP, Vol. 8		1966
Annual Report, Osaka Lab., No. 1	JAERI 5018	1967
Annual Report, Osaka Lab., No. 2	JAERI 5022	1968
Annual Report, Osaka Lab., No. 3	JAERI 5026	1969
Annual Report, Osaka Lab., No. 4	JAERI 5027	1970
Annual Report, Osaka Lab., No. 5	JAERI 5028	1971
Annual Report, Osaka Lab., No. 6	JAERI 5029	1972
Annual Report, Osaka Lab., No. 7	JAERI 5030	1973
Annual Report, Osaka Lab., No. 8	JAERI-M 6260	1974
Annual Report, Osaka Lab., No. 9	JAERI-M 6702	1975
Annual Report, Osaka Lab., No.10	JAERI-M 7355	1976
Annual Report, Osaka Lab., No.11	JAERI-M 7949	1977
Annual Report, Osaka Lab., No.12	JAERI-M 8569	1978
Annual Report, Osaka Lab., No.13	JAERI-M 9214	1979
Annual Report, Osaka Lab., No.14	JAERI-M 9856	1980
Annual Report, Osaka Lab., No.15	JAERI-M 82-192	1981
Annual Report, Osaka Lab., No.16	JAERI-M 83-199	1982
Annual Report, Osaka Lab., No.17	JAERI-M 84-239	1983
Annual Report, Osaka Lab., No.18	JAERI-M 86-051	1984

* Year of the activities

Keywords: Electron Beam Irradiation, γ-Irradiation, Radiation Induced Reaction, Polymerization, Grafting, Polymer Modification, Polystyrene, Radiation Chemistry, Auger Spectrum, Titanium Carbide, Silicon Carbide, Adsorption, Ion Impact Desorption, Fischer-Tropsch Reaction.

昭和60年度日本原子力研究所大阪支所年報（No.19）
1985年4月1日 ～ 1986年3月31日

日本原子力研究所高崎研究所大阪支所

（1987年2月18日受理）

本報告書は、大阪支所において昭和50年度に行われた研究活動を述べたものである。主な研究題目は、電子及びイオン照射下の界面現象に関する基礎研究、電子線照射による重合反応の研究、ポリマーの改質及び上記の研究と関連して重合反応、高分子の分解及び架橋ならびにグラフト重合に関する基礎的な研究などである。

日本放射線高分子研究協会年報	Vol. 1		1958／1959
日本放射線高分子研究協会年報	Vol. 2		1960
日本放射線高分子研究協会年報	Vol. 3		1961
日本放射線高分子研究協会年報	Vol. 4		1962
日本放射線高分子研究協会年報	Vol. 5		1963
日本放射線高分子研究協会年報	Vol. 6		1964
日本放射線高分子研究協会年報	Vol. 7		1965
日本放射線高分子研究協会年報	Vol. 8		1966
日本原子力研究所大阪研における放射線化学の基礎研究No.1	JAERI	5018	1967
日本原子力研究所大阪研における放射線化学の基礎研究No.2	JAERI	5022	1968
日本原子力研究所大阪研における放射線化学の基礎研究No.3	JAERI	5026	1969
日本原子力研究所大阪研における放射線化学の基礎研究No.4	JAERI	5027	1970
日本原子力研究所大阪研における放射線化学の基礎研究No.5	JAERI	5028	1971
日本原子力研究所大阪研における放射線化学の基礎研究No.6	JAERI	5029	1972
日本原子力研究所大阪研における放射線化学の基礎研究No.7	JAERI	5030	1973
Annual Report, Osaka Lab., JAERI, No.8	JAERI-M	6260	1974
Annual Report, Osaka Lab., JAERI, No.9	JAERI-M	6702	1975
Annual Report, Osaka Lab., JAERI, No.10	JAERI-M	7355	1976
Annual Report, Osaka Lab., JAERI, No.11	JAERI-M	7949	1977
Annual Report, Osaka Lab., JAERI, No.12	JAERI-M	8569	1978
Annual Report, Osaka Lab., JAERI, No.13	JAERI-M	9214	1979
Annual Report, Osaka Lab., JAERI, No.14	JAERI-M	9856	1980
Annual Report, Osaka Lab., JAERI, No.15	JAERI-M	82-192	1981
Annual Report, Osaka Lab., JAERI, No.16	JAERI-M	83-199	1982
Annual Report, Osaka Lab., JAERI, No.17	JAERI-M	84-239	1983
Annual Report, Osaka Lab., JAERI, No.18	JAERI-M	86-051	1984

大阪支所：大阪府寝屋川市三井南町25の1

CONTENTS

1. INTRODUCTION

Osaka Laboratory was founded in 1958 as a laboratory of the Japanese Association for Radiation Research on Polymers (JARRP), which was organized and sponsored by some fifty companies interested in radiation chemistry of polymers. The JARRP was merged with Japan Atomic Energy Research Institute (JAERI) on June 1, 1967, and the laboratory has been operated as Osaka Laboratory for Radiation Chemistry, Takasaki Radiation Chemistry Establishment, JAERI. The research activities of Osaka Laboratory have been oriented towards the fundamental research on applied radiation chemistry.

The studies on electron- and ion-impact induced adsorption and desorption of gases on solid surfaces are important since they will help understand the phenomena occurred on the first wall surface of present-day and future nuclear fusion reactors.

Studies have been carried out on adsorption and desorption of oxygen on the surface of TiC/Inconel and TiC/Mo which are currently employed as the first wall materials of JT-60, and of silicon carbide(SiC). Adsorption of oxygen was found to occur selectively on the carbon atoms of the TiC surface, and on the silicon atoms of the SiC surface, respectively. The desorption cross sections of oxygen on TiC/Inconel and SiC by Ar^+ impact increased slightly with the incident ion energy, whereas those by H_2^+ and D_2^+ decreased at higher ion energies.

Study to prepare chemically active or inactive surface by electron beam recoil doping on solid surfaces has been continued on polyimide surface and iron as injecting element. It was found that iron was implanted 300 nm below the surface from the change in Auger spectrum during argon ion sputtering, when polyimide surface was irradiated with 800 keV electrons in the atmosphere of Ar-iron pentacarbonyl mixture.

Grafting of acrylic acid onto high density polyethylene

film was carried out in order to elucidate the relation between the distribution of grafted layer and the grafting conditions and it was found that the surface morphology and depth distribution of the polyacrylic acid greatly depend on the grafting conditions.

The study of the structure of nylon 66 film of various history of thermal treatments and electron irradiation has continued in an attempt to obtain polymer films of different surface structures on which the studies on thin layer grafting are to be carried out. Nylon 66 films of different crystallinities have been obtained by electron beam irradiation of the film.

In the study to assign the thermoluminescence centers of polymeric materials for understanding coloration mechanism of film dosimeters, it was found that some of the thermo-luminescence peaks appeared at different temperature regions in low density polyethylene were accompanied by the thermo-stimulationg current.

Sad news arrived us in the morning of June 23rd, 1986 that Professor Ichiro Sakurada, the Emeritus Professor of Kyoto University and a member of the Japan Academy awarded as the nation's highest honorable scholor (1977), died at the age of 82. He directed the research as director from 1958 and then from 1967 when the Laboratory was merged to JAERI until his retirement in 1975. He further contributed to keep the research activities at high levels as a research advisor until 1981. It was he that established the basis of all research activities carried out or being carried out in this laboratory. We are very much indebted to his outstanding service for our research with strong encouragement and kind advice.

January 27th, 1987

Dr. Motoyoshi Hatada, Director
Osaka Laboratory for Radiation Chemistry
Japan Atomic Energy Research Institute

II. RECENT RESEARCH ACTIVITIES

1. Oxygen on TiC: Adsorption and Ion Impact Desorption

Since oxygen is one of the main plasma impurities in tokamaks,[1] it is important to study surface processes involving oxygen such as retention and desorption on first wall materials. Described below are the results obtained for adsorption and desorption of oxygen occurring during electron and ion impact on TiC coating materials that are currently used for the first wall in JT-60.

Experiments were carried out using the same apparatus described previously[2] except that a commercial ion gun (Perkin-Elmer, PHI Model 04-303) was replaced with that used before. TiC samples used in this study were thin films (20 μm) coated on Inconel 625 and Mo which were kindly donated from Plasma Eng. Lab., Dept. of Thermonuclear Fusion Res., Naka Fusion Res. Estab., JAERI. The surface of the samples was cleaned by bombarding with 4 keV Ar^+ ions, whereupon the Auger spectrum showed no signals due to oxygen and other impurities. Adsorption of oxygen on and its desorption from the surface were monitored by Auger electron spectroscopy (AES). Auger spectra were recorded using electron beams of 1.5 keV and 20 μA. O_2 (Seitetsu Kagaku, 99.995 % up) was admitted to the chamber through a variable leak valve. The ions used for desorption were 1 ∿ 5 keV Ar^+, H_2^+, and D_2^+. Atomic concentrations on the surface were determined from AES data using the following sensitivity factors determined in this study: 0.20 for C(KLL), 0.11 for Ti($L_{23}M_{23}M_{23}$) and 0.30 for O(KLL).

The atomic surface concentration ratios, C/Ti for TiC/Inconel and TiC/Mo after Ar^+ bombardment were 0.96±0.01 and

1.03±0.02, respectively. On exposure of the surface to O_2 at a constant pressure, O(KLL) signal appears immediately in the Auger spectrum and grows in intensity with time. Figure 1

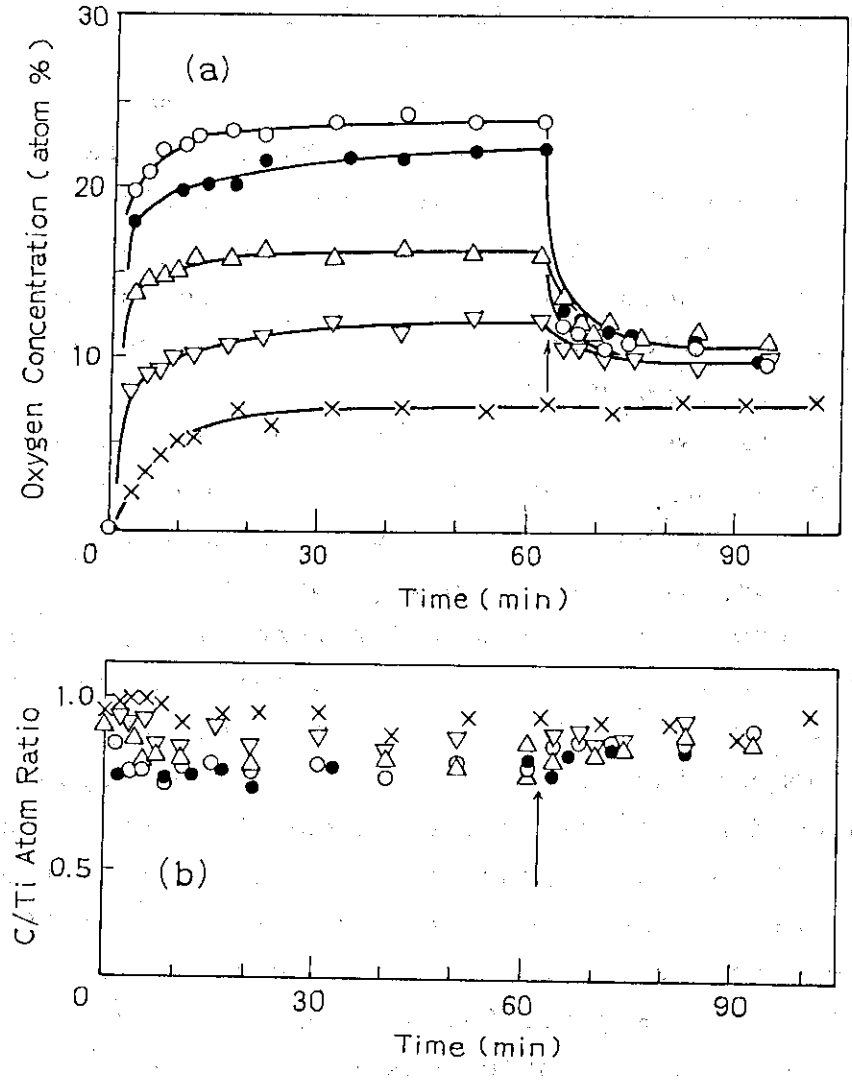

Fig. 1 Oxygen concentration (a) and C/Ti atom ratio (b) during electron impact on TiC/Inconel in oxygen atmosphere and in UHV. Arrows indicate the time when oxygen supply was stopped. (○); 1×10^{-6} Torr O_2, (●); 5×10^{-7} Torr O_2, (△); 1×10^{-7} Torr O_2, (▽)2×10^{-8} Torr O_2, (×); in UHV.

shows variation of oxygen concentration and C/Ti ratio with time for TiC/Inconel in four different O_2 pressures and in UHV. The oxygen concentration in each case reaches a stationary value after 20 min, the value being greater at higher oxygen pressure. When O_2 supply was stopped and the O_2 in the chamber was pumped out, the oxygen concentration decreases rapidly to approach the stationary concentration obtained when electron impact was continuously carried out in UHV from the beginning. The increase of the oxygen concentration in O_2 is accompanied with the decrease in the concentrations of both C and Ti atoms. The decrease of the concentration of C atoms is greater than that of Ti, which results in the decrease in C/Ti ratio (Fig. 1b), the extent of the decrease being greater at higher O_2 pressures. The behavior of the C/Ti ratio when O_2 supply was stopped is the same as that of the oxygen concentration. Similar results were obtained for TiC/Mo as shown in Fig. 2.

The dependence of the oxygen stationary concentration on the ambient O_2 pressure suggests that the concentration of surface oxygen is in an equilibrium with that in gas phase. The fact that C/Ti ratio decreases with the increase of the surface oxygen concentration indicates that oxygen is preferentially adsorbed on C atoms on the surface. This agrees well the previous work on oxygen chemisorption on TiC(001).[3]

Ion impact desorption data were obtained for TiC/Inconel. After the surface oxygen concentration reached ca. 10 atomic % by exposure to 5×10^{-7} Torr of O_2 for 10 min followed by pumping out of the O_2, TiC/Inconel surface was bombarded with either Ar^+, H_2^+, or D_2^+. The concentration of surface oxygen (n) was found to decrease exponentially with time of ion bombardment. Ion impact desorption cross section (Q) was obtained from plots of this time dependence according to eq. 1, where n_0 and n_∞ are

$$(n - n_\infty)/(n_0 - n_\infty) = -\exp\{-(JQ/\varepsilon)\}t \qquad (1)$$

the initial and final concentrations of surface oxygen, and J and ε are the current density and charge of primary ions, respectively. The results are shown in Fig. 3. The cross sections due to Ar^+ ion impact obtained here are in a good agreement with 5.0×10^{-16} cm^2 (at 1 keV) $\sim$ 6.2×10^{-16} cm^2 (5 KeV) reported for oxygen adsorbed on TiC/graphite.[4] It is noted that the energy dependence of the cross sections is different from that due to H_2^+ and D_2^+ ion impact. Effort is continued to establish a model to obtain the cross sections due to impact with various ions.

(S. Nagai)

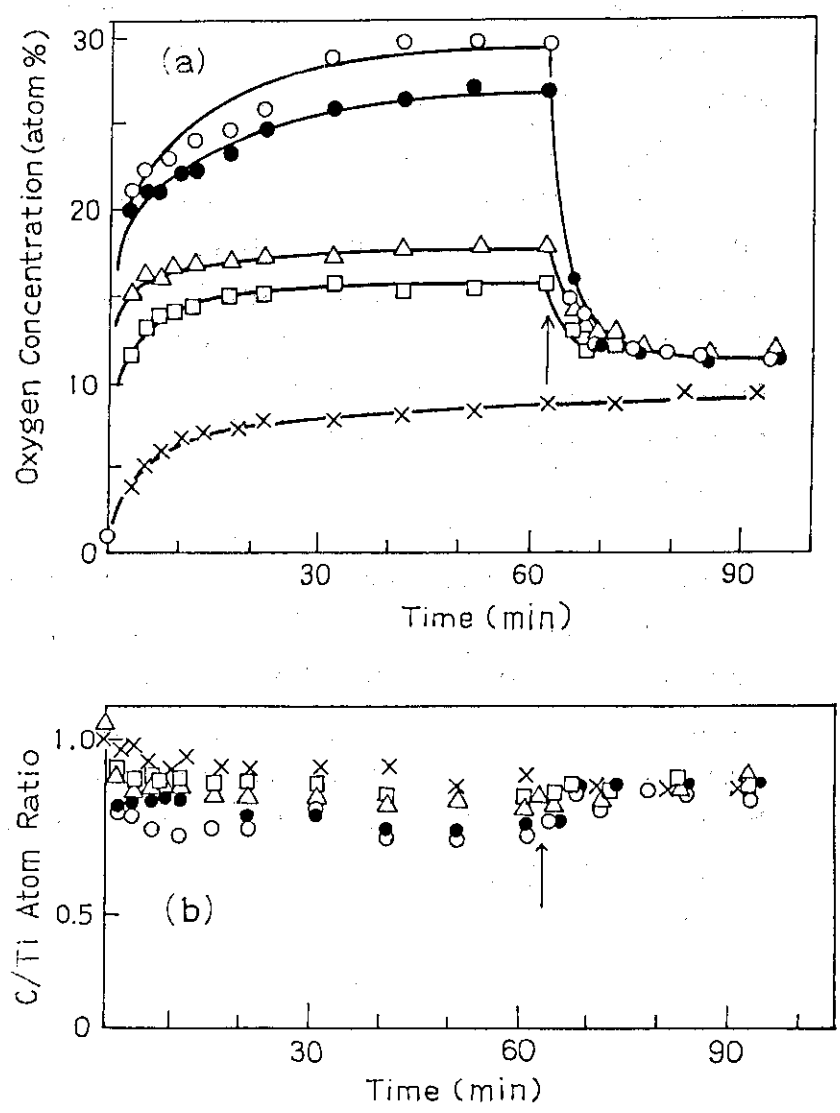

Fig.2 Oxygen concentration (a) and C/Ti atom ratio (b) during electron impact on TiC/Mo in oxygen atmosphere and in UHV. Arrows denote the time when oxygen supply was stopped. (○); 1 x 10^{-6} Torr O_2, (●); 5 x 10^{-7} Torr O_2, (△); 1 x 10^{-7} Torr O_2, (□); 5 x 10^{-8} Torr O_2, (×); in UHV.

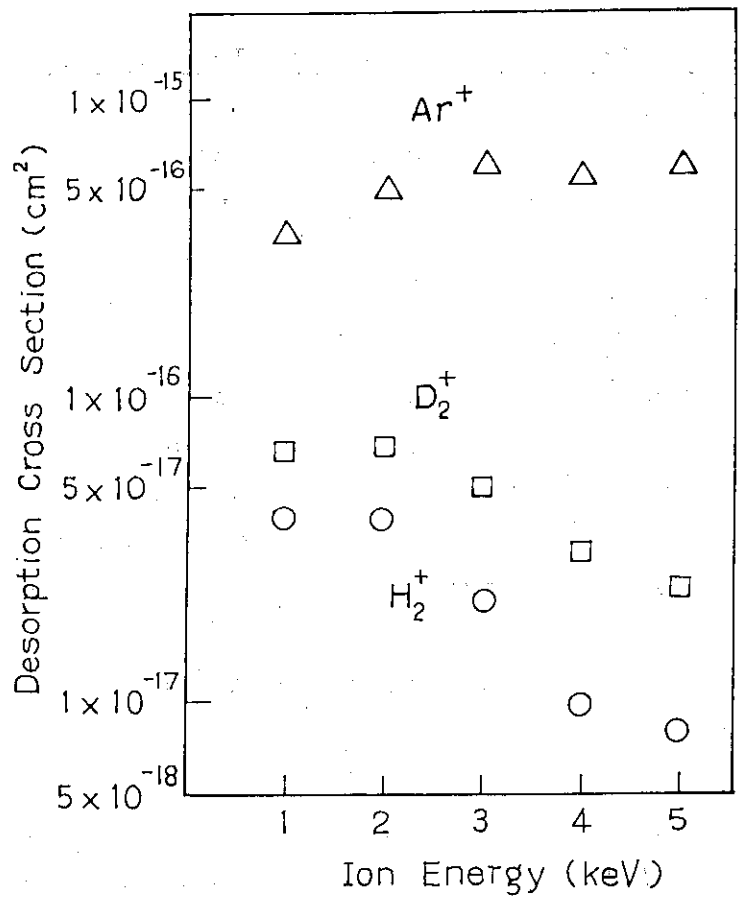

Fig. 3 Experimental ion impact desorption cross sections of oxygen from TiC/Inconel.

1) W. R. Wampler and D. K. Brice, J. Vac. Sci. Technol., A4, 1186(1986) and references therein.
2) S. Nagai and Y. Shimizu, J. Nucl. Mat., 128/129, 605(1984).
3) C. Oshima, M. Aono, T. Tanaka, S. Kawai, S. Zaima and Y. Shibata, Surf. Sci., 102, 312(1981).
4) S. Sukenobu and Y. Gomay, J. Nucl. Mat., 128/129, 775(1984).

2. Oxygen on SiC: Adsorption and Ion Impact Desorption

Studies have been carried out of adsorption and desorption of oxygen on silicon carbide (SiC). Since SiC is thought of as one of the favored candidates for the first wall materials of fusion devices, several studies on SiC have already been carried out from a viewpoint of plasma surface interactions.[1] However, no studies have yet been made on adsorption and desorption processes of gases on the surface.

The apparatus and experimental procedures are the same as in the preceding account of this report. Single crystal of α-SiC grown at National Inst. for Res. in Inorg. Materials was used here.

The Auger spectrum of SiC after Ar^+ bombardment consists of Si(LVV) and C(KLL) in addition to weak Ar(LVV) due to implanted Ar^+ ions. When the SiC surface was continuously bombarded with electrons in UHV to record the Auger spectrum, the intensity of Si(LVV) decreases gradually with time and finally levells off as shown in Fig. 1. C(KLL) remains unchanged both in shape and intensity. On the other hand, O(KLL) appears at the early stage of this electron impact and grows in intensity with time.

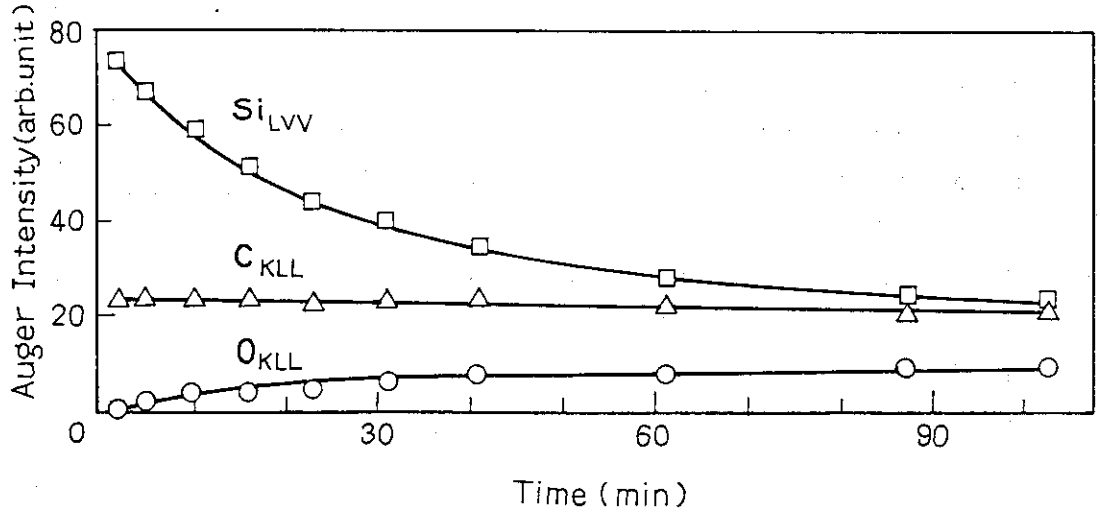

Fig. 1 Change in Auger intensity for SiC during electron impact in UHV.

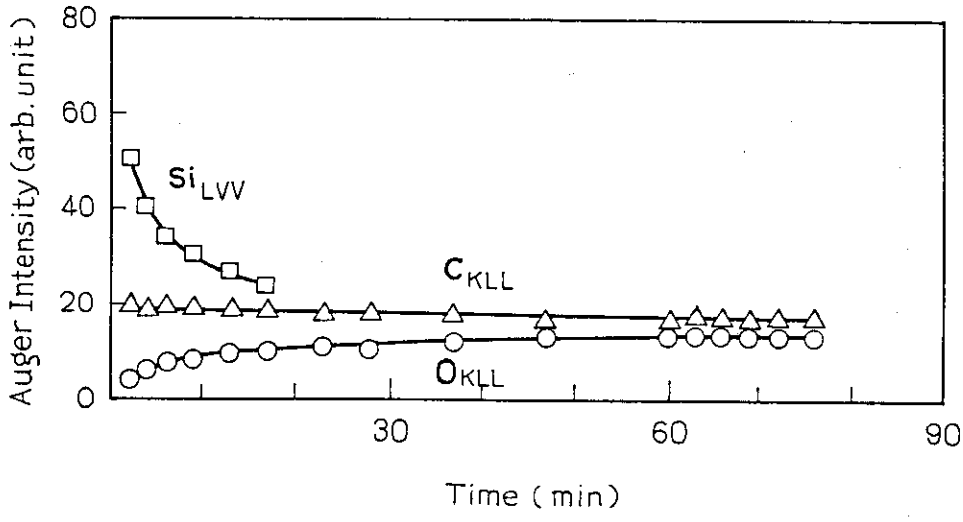

Fig. 2 Change in Auger intensity for Sic during electron impact in 5×10^{-8} Torr of O_2.

Figure 2 shows a similar plot for the change of the Auger intensities of the three signals observed during a continuous electron impact on the surface in 5×10^{-8} Torr of oxygen. Si(LVV) decreases in intensity more rapidly than in UHV and broadens in width after ca. 20 min. though the peak energy shows no shift from original 93 eV. The behaviors of C(KLL) and O(KLL) each are similar to those in UHV except that the intensity of O(KLL) becomes greater than in UHV.

When the ambient pressure of oxygen during electron impact was increased to 1×10^{-7} Torr, the Auger spectrum sustains further changes. Figure 3 and 4 show changes in Auger spectrum and in the intensity, respectively, in 5×10^{-7} Torr of oxygen. It can be seen from Fig. 3 that Si(LVV) rapidly decreases in intensity to disappear almost completely. Since the final peak

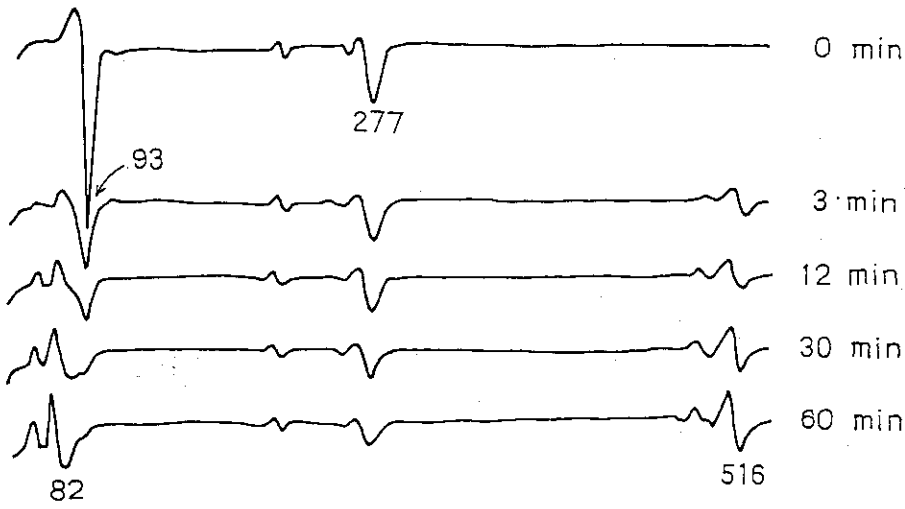

Fig. 3 Change of Auger spectrum of SiC during electron impact in 5 x 10^{-7} Torr of O_2.

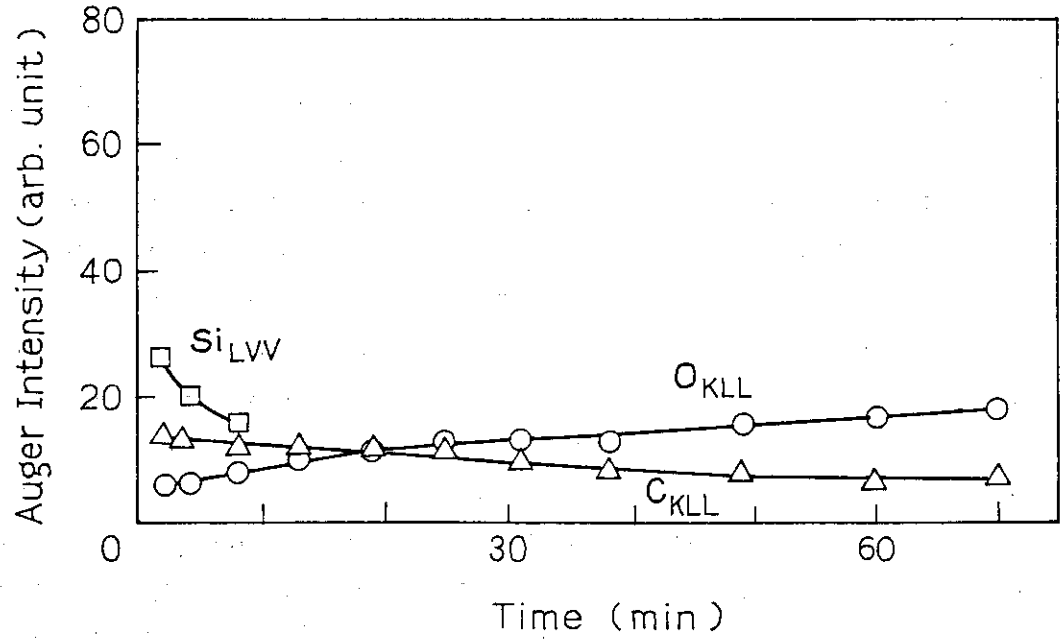

Fig. 4 Change in Auger intensity for SiC during electron impact in 5 x 10^{-7} Torr of O_2.

energy, 82 eV is identical with that of a well known silicon oxide, this spectral change means a conversion of SiC to SiO_2. It is noted that this change is accompanied by not only the growth of O(KLL) but also the decrease of C(KLL) intensity, that is not observed at lower O_2 pressures.

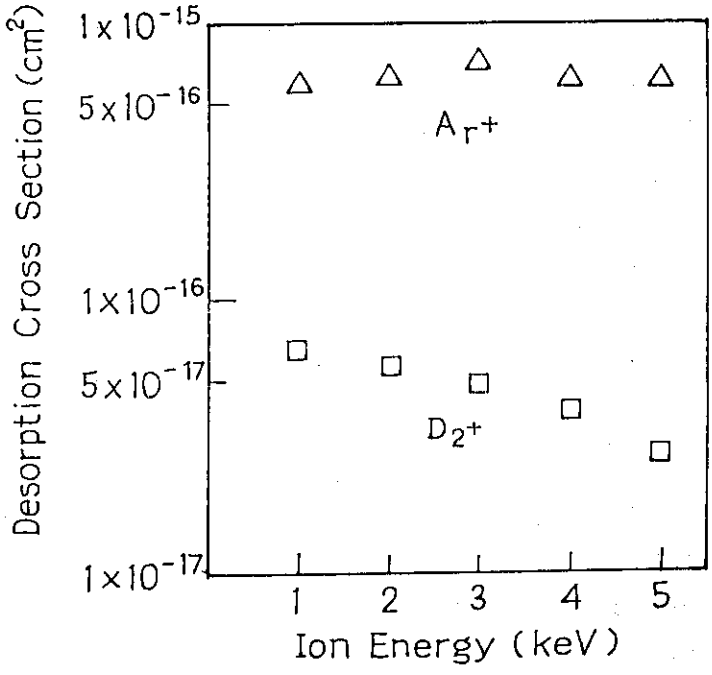

Fig. 5 Experimental desorption cross sections of oxygen on SiC.

These results indicate that adsorption of oxygen on the SiC surface takes place preferentially on Si sites at low surface coverage while it occurs on the whole surface involving oxidation of Si atoms on the surface at high coverage.

Desorption cross sections of oxygen by Ar^+ and D_2^+ ion impact are shown in Fig. 5 as a function of the primary ion energy. The cross sections by Ar^+ are $5.9 \sim 7.1 \times 10^{-16}$ cm^2 in the range of 1 5 keV, not very dependent on the ion energy. Those by D_2^+ decrease with the ion energy and are close to those obtained for oxygen on TiC/Inconel in the preceding paper.

(S. Nagai)

1) S. Adachi, M. Mohri and T. Yamashina, Surface Sci., 161, 479(1985).

3. Preparation of Carbon Films by R.F. Glow Discharge Method

Recently, much attention has been given to hard carbon films, so-called diamond-like carbon or i-C films in view of their some remarkable properties such as electrical insulating, extreme hardness, optical characteristics, and chemical inertness.[1] R.F. glow or micro-wave discharge and ion beam techniques have been employed to prepare such carbon films. It is well known that growth rate and properties of the films prepared by plasma glow discharge are significantly affected, not only by reaction conditions such as reaction time, temperature and gas composition but also, by type of reactor used and by generating conditions of plasma.[2] In order to prepare the hard carbon films as specimens for studying on adsorption and desorptipn of gases on its surface, studies were carried out here on the effects of flow rate, methane concentration, r.f. power and electrode-electrode distance from gaseous mixture of methane and hydrogen by the plasma glow discharge method. Some properties of the films obtained were checked by electrical, thermal and spectroscopic measurements.

Figure 1 shows the experimental apparatus (Samco Co., model BP-1) used for preparation of carbon films. The reactor was of a capacitively coupled parallel-electrode, inner electrode- and bell jar-type. The power supply for generation of plasma is used in a r.f. 13.56 MHz oscillator. Pyrex glass plate of the size 40 × 15 × 1.0 mm^3 was mainly used here as substrates, and in some cases nickel or aluminum plates were used. These substrates were cleaned by washing with a 10% alkaline cleaning liquid, distilled water and methyl alcohol followed by drying at about 140°C before usage. The substrates were placed on a lower electrode(cathode) of 100 mm in diameter. After the reactor was evacuated to a pressure below 2×10^{-2} Torr, gaseous mixture of methane and hydrogen was

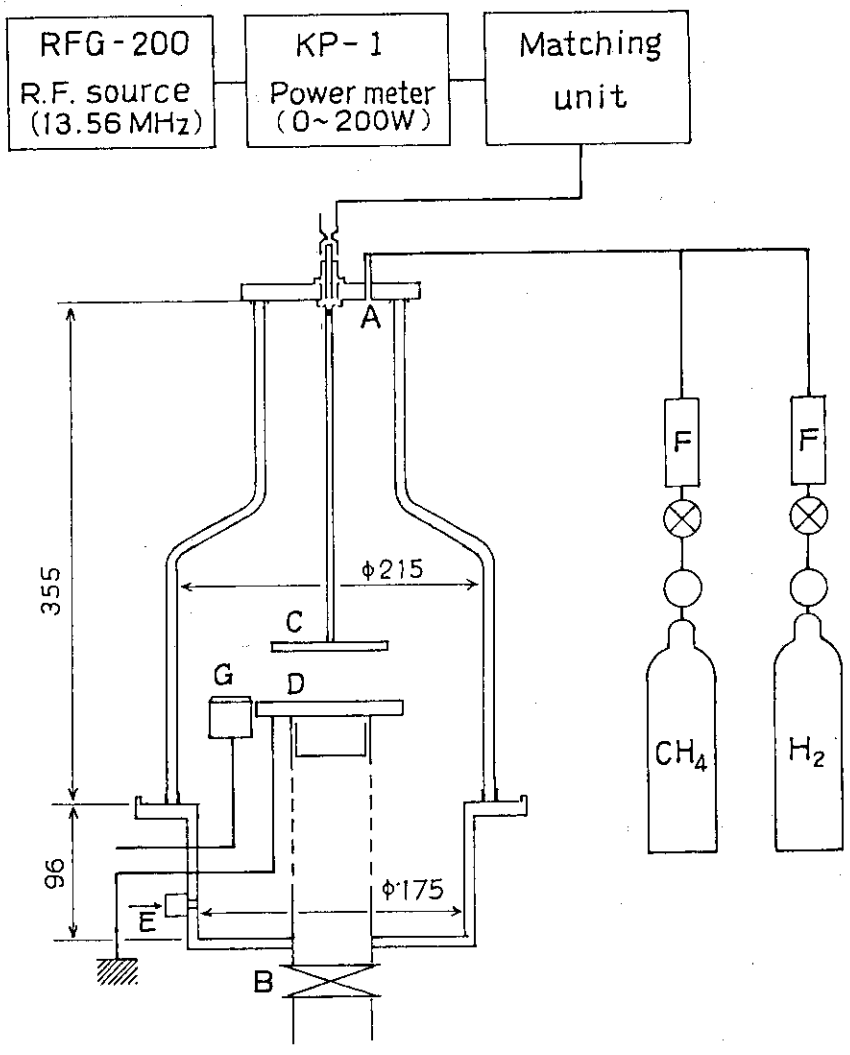

Fig. 1 Experimental apparatus for the preparation of carbon films.
A, Gas inlet; B, Vacuum pump; C, Upper electrode;
D, Lower electrode; E, Pressure gauge; F, Flow meter;
G, Thickness sensor.

introduced into the reactor through the flowmeters. The total flow rate of the mixed gas was 15 ∿ 64 cm^3 min^{-1} at room temperature. The pressure in the reactor, ca. 0.5 ∿ 2.6 Torr, was measured with a thermocouple gauge. The substrate temperature was always about 180°C.

The following reaction conditions were found to be suitable to prepare uniform carbon films: total flow rate; 61 cm^3 min^{-1}, methane concentration; 16.7%, power of r.f; 100 W, electrode-electrode distance, 15 mm, and reaction time; 138 min. In all the flow rates from 15 to 64 cm^3 min^{-1}, uniform carbon films were obtained when the other parameters were fixed as above. Figure 2 shows the effects of methane concentration and reaction time on the deposition of carbon films. Uniform deposition of films was observed with the methane concentration of 0.55 ∿ 41% for the reaction time of

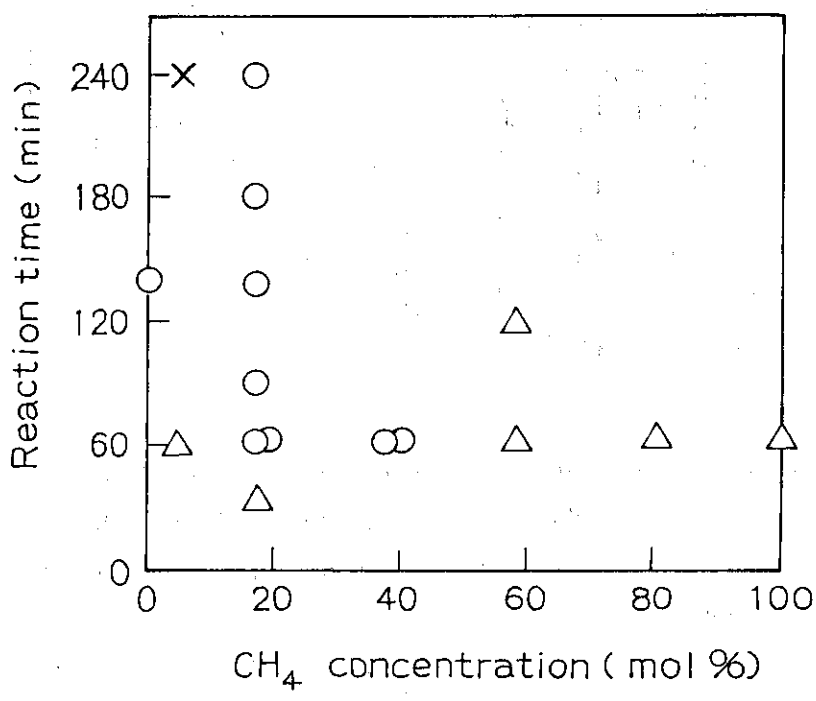

Fig. 2 Effects of methane concentration and reaction time on the deposition of carbon films onto Pyrex glass. Symbols show uniform(○) and partial(△) deposition of the films, and no deposition(×). Total flow rate 61 cm^3/min; r.f. power, 100 W; electrode-electrode distance, 15 mm.

60 min or more. On the other hand, carbon films were only partially deposited on the substrate with the methane concentration of 58.5 ∿ 100%, accompanied with the formation of large amounts of soot-like carbon. Figure 3 shows the effect of r.f. power. As seen in the figure, carbon films were uniformly deposited on glass substrate with r.f. power of 50 ∿ 150 W.

The carbon films prepared at the reaction conditions described above, exhibit yellowish or brownish hue. The thickness of the films on glass substrate was about 1600 Å.

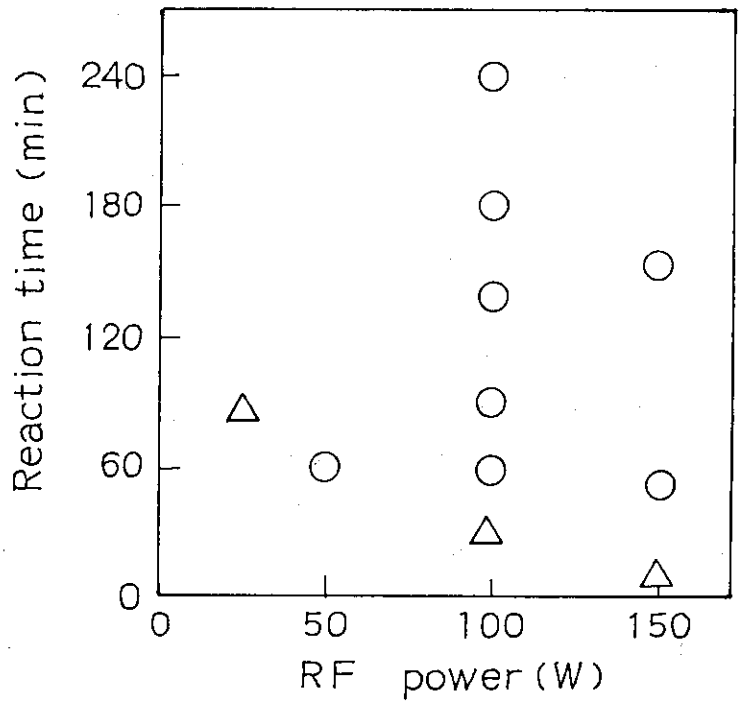

Fig. 3 Effect of r.f. power on the deposition of carbon films onto Pyrex glass. Symbols as in fig. 2. Total flow rate, 61 cm^3/in; methane concentration, 16.7%; electrode-electrode distance, 15 mm.

Thermal property of the films was measured using DSC apparatus (Rigaku Denki, type DSC 10 A) for the samples(ca. 0.2 mg) that had been exposed to N_2 atmosphere for about 60 min (at ca. 12% humidty). Figure 4 shows DSC curve of the carbon films prepared, with the curve of high density polyethylene (Asahi Chemicals Co.). Although polyethylene shows a sharp peak due to melting at 128°C, the carbon films show no peaks up to about 270°C, indicating that the carbon films have higher melting point than polyethylene.

The electric conductivity of the carbon films deposited onto nickel substrate was measured by a two-probe method at room temperature using Keithley-616-digital electrometer. The specific resistance of the films showed about 10^{11} Ωcm. This value points to be smaller than that of natural diamond(type I) (10^{16} Ωcm),[3] but almost identical with that of diamond-like carbon films.[4]

Figure 5 shows infrared absorption spectrum of carbon films prepared onto glass plate coated with aluminum thin films. As shown, the carbon films gave strong absorption peaks at 2950, 2870, 1440, 1370 and 2925 cm^{-1} due to methyl and methylene groups. The absorption peaks lying from 1600 to 1700 cm^{-1} may be assigned to either alkene, unsaturated carbonyl group or CO_2 adsorbed on the films. The spectrum in the range of 3000 ∿ 2800 cm^{-1} is similar to that of amorphous carbon film reported by Haba et al.[5] These results indicate that the carbon films contain significant amounts of hydrogen in the structure, in agreement with the work by Mirtich et al.[6] in which amorphous carbon films contain a large amount of hydrogen in the structure(H/C≃1.00).

X-ray diffraction pattern of carbon films prepared onto glass plate was recorded with an X-ray diffraction apparatus (Geiger flex, D-S type, Rigaku Denki) using nickel filtered copper Kα radiation of 30 kV, 20 mA.

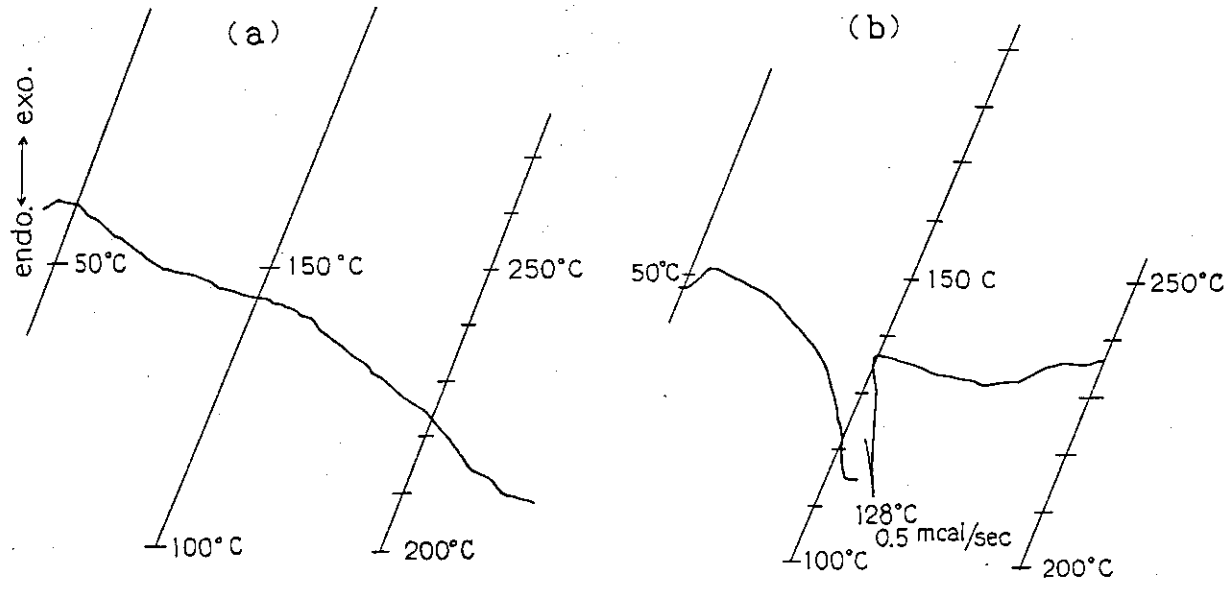

Fig. 4 DSC curves of carbon films(a) and high density polyethylene(b). Sample(a): total flow rate, 61 cm^3/min; methane concentration, 16.7%; r.f. power, 100 W; electrode-electrode distance, 15 mm; reaction time, 138 min. Analytical conditions: weight, ca. 0.2 mg; sensitivity, ±0.25 mcal/sec; heating rate, 100 °C/min.

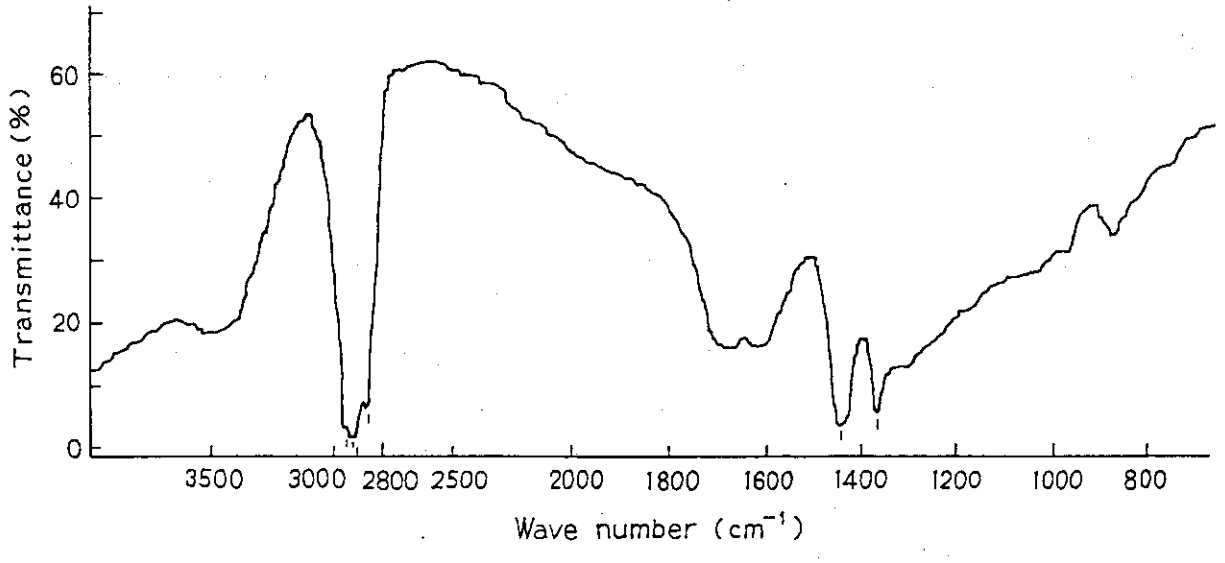

Fig. 5 IR reflection-absorption spectrum of carbon films. Reaction conditions: total flow rate, 61 cm^3/min; methane concentration, 16.7%; r.f. power, 100 W; electrode-electrode distance, 15 mm; reaction time, 138 min.

As shown in Fig. 6, X-ray diffraction pattern of the films shows weak peaks at around 2θ=75, 42 and 28°. Another diffraction peak was also observed at around 2θ=94° though being very weak. It is well known that the diffraction peaks at 2θ=44, 75 and 91.5° are due to the polycrystalline diamond structure.[7] Accordingly, this result shows that the carbon films have at least some polycrystalline diamond structure. Further study is under way to prepare diamond thin films with good crystallinity.

(Y. Shimizu and S. Nagai)

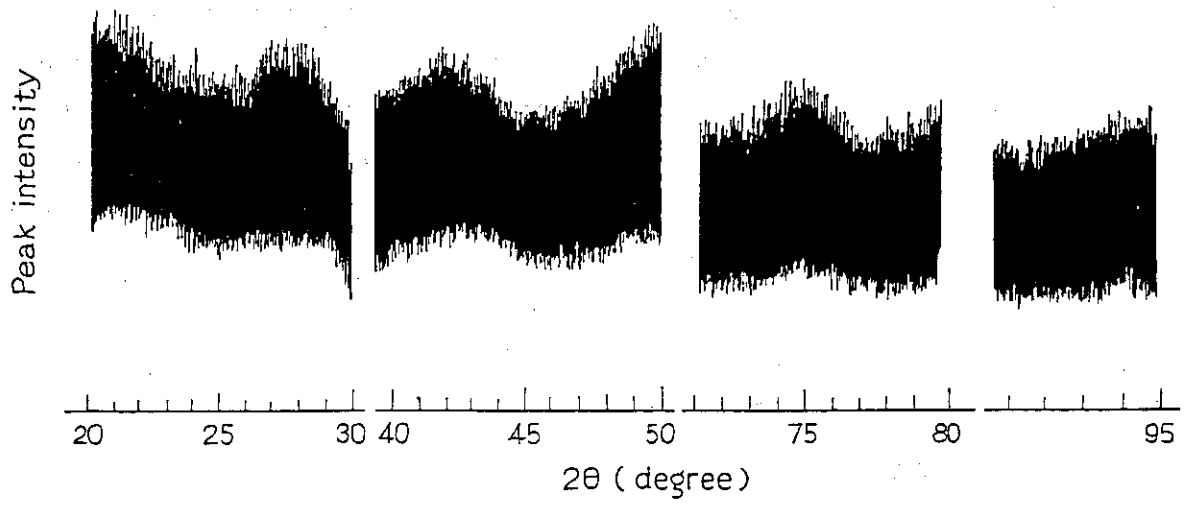

Fig. 6 X-ray diffraction pattern of carbon films. Reaction conditions: total flow rate, 61 cm^3/min; methane concentration, 16.7%; r.f. power, 100 W; electrode-electrode distance, 15 mm; reaction time, 138 min. Analytical conditions: 30 kV, 20 mA.

1) Some examples in L. P. Anderson, Thin Solid Films. 86, 193 (1981).
2) Some examples in S. M. Ojha, H. Norstrom and D. Mcculluch, Thin Solid Films, 60, 213(1979).
3) Some examples in T. Hayashi, T. Imura and M. Hirose, Proceeding of the 9th symposium on Ion Source and Ion-Assisted Technology, Tokyo(1985) 247.
4) K. Kobayashi, N. Mutsukura and Y. Machi, ibid., 251.
5) M. Haba, M. Watanabe, M. Hayashi and Y. Tagawa, ibid., 265.
6) M. J. Mirtich, D. M. Swec and J. C. Angus, Thin Solid Films, 131, 245(1985).
7) Some examples in Y. Satoh, M. Kamo and N. Sedaka, Proceeding of the 9th symposium on Ion Source and Ion-Assisted Technology Tokyo(1985) 223.

4. Catalytic Activity for Fischer-Tropsch Reaction on the Kapton Film Electron-Beam Doped with Iron

In the last annual report,[1] we reported that Kapton film(Kapton 500 H) which had been irradiated with 0.8 MeV electrons under the presence of gas mixture containing Ar and $Fe(CO)_5$ showed catalytic activity for Fischer-Tropsch reaction and also showed that Fe was implanted in the surface region by the irradiation by AES method.[1] This year, we prepared four Kapton samples: (I) Kapton film was irradiated under the presence of Ar-$Fe(CO)_5$ gas mixture and then iron deposited on the film surface was removed with 0.1 N HCl solution as described in the previous report; (II) the same procedure except that iron was deposited without irradiation by thermal decomposition from the gas mixture; (III) iron was deposited on the film by vaccum evaporation at the surface concentrataion of

0.2 mg/cm^2; and (IV) after irradiation of the film(III), iron deposited on the surface was removed by 0.1 N HCl as done in (I). Silica gel catalyst was also prepared for reference purpose by the same method as (I).

The methods of irradiation, and measurements of catalytic activity and of depth profile of the samples were the same as those described in the previous report.[1)]

The depth profile of sample(I) is shown in Fig. 1, where it is shown that iron was found even ca. 300 nm below the surface. Since the projection range of Fe^+ implanted assisted with 800 keV electrons in Kapton is calculated to be several tenths of nm,[1)] the depth found in this study is far deeper than that expected. Diffusion assisted energetic electrons in Kapton might be accounted for this unexpected large depth as suggested by Wada in the electron assisted doping at aluminum-silicon interface.[2)] Decrease of O atom and increase

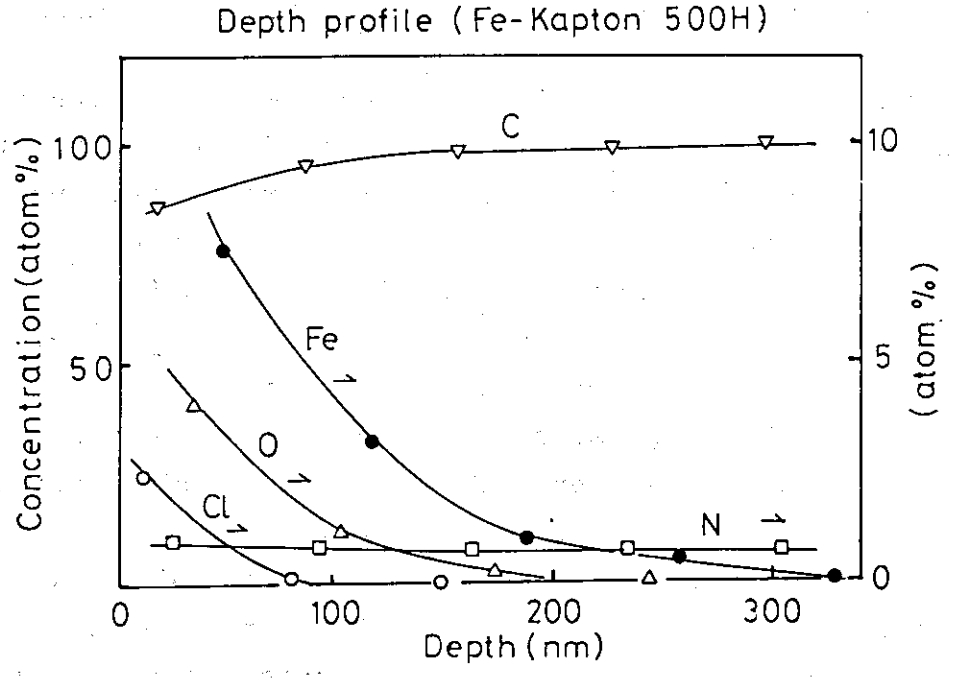

Fig. 1 Depth profile of elements.

of C atom concentrations with depth indicate that carbonization, possibly, graphitization proceeds during sputtering.

In Table 1, the rate of products formation and the relative amounts of the products are shown for the five samples. As shown in the Table, samples (I),(III) and (V) showed activity. Thus, the irradiation of Kapton in the presence of iron in the gas phase seems to be important to deposit iron in some depth from the surface of Kapton for catalytic activity. The reason why iron was not implanted from solid iron into Kapton (i.e. no activity on sample IV) is not clear but may be due to that the electron energy of 0.8 MeV is not enough to knock out iron atoms from solid iron crystal lattice. It is noted that the relative amount of C_2H_4 to C_2H_6 on (I) is 10 times larger than that on (III) and (V) showing strong selectivity to ethylene formation.

In Fig. 2, the rates of hydrocarbon formation are plotted as a function of beam current, electron accelerating voltage being kept constant at 0.8 MV.; the temperature during

Table 1 Catalytic activity* of Fe-implanted Kapton at 304°C

Kapton		CH_4	C_2H_4	C_2H_6	C_3H_6
(I)	Fe-implanted	0.017	0.0045	0.0002	0.0014
		(72.3)**	(18.6)	(0.8)	(5.3)
(II)	Fe-therm.deposn.	0.0008	0.0001	--	--
(III)	Fe-evaporated	0.22	0.028	0.016	0.014
		(71.6)	(9.2)	(5.4)	(4.6)
(IV)	Irradiated Silica gel	0.0006	0.0001	--	--
(V)	Fe-implanted	(60.3)	(13.5)	(6.3)	(9.5)

*) $\mu mol \cdot 1 reactant^{-1} \cdot 10 cm^2 Kapton^{-1} \cdot min^{-1}$

**) Hydrocarbon content (%)

irradiations also shown on the upper scale. As shown in Fig. 2, the rates are almost independent of beam current in the range from 0.25 mA to 3 mA and then increased sharply with increasing beam current.

The rates of hydrocarbon formation are plotted as a function of temperature at 0.8 MV and 2 mA in Fig. 3, where it is clear that the rates increased with increasing temperature up to 200°C and then levelled off above 200°C. Thus, a sharp increases of the rates at beam current of 3 mA (Fig. 2) are more than those expected from the effects of temperature on the

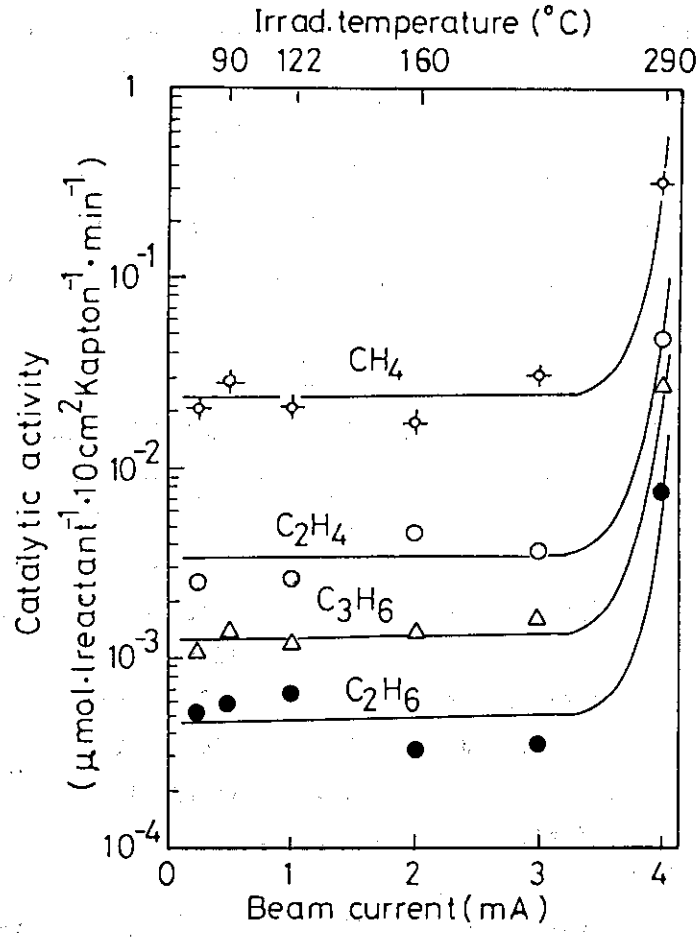

Fig. 2 Relation between catalytic activity and beam current of electron-beam doping.

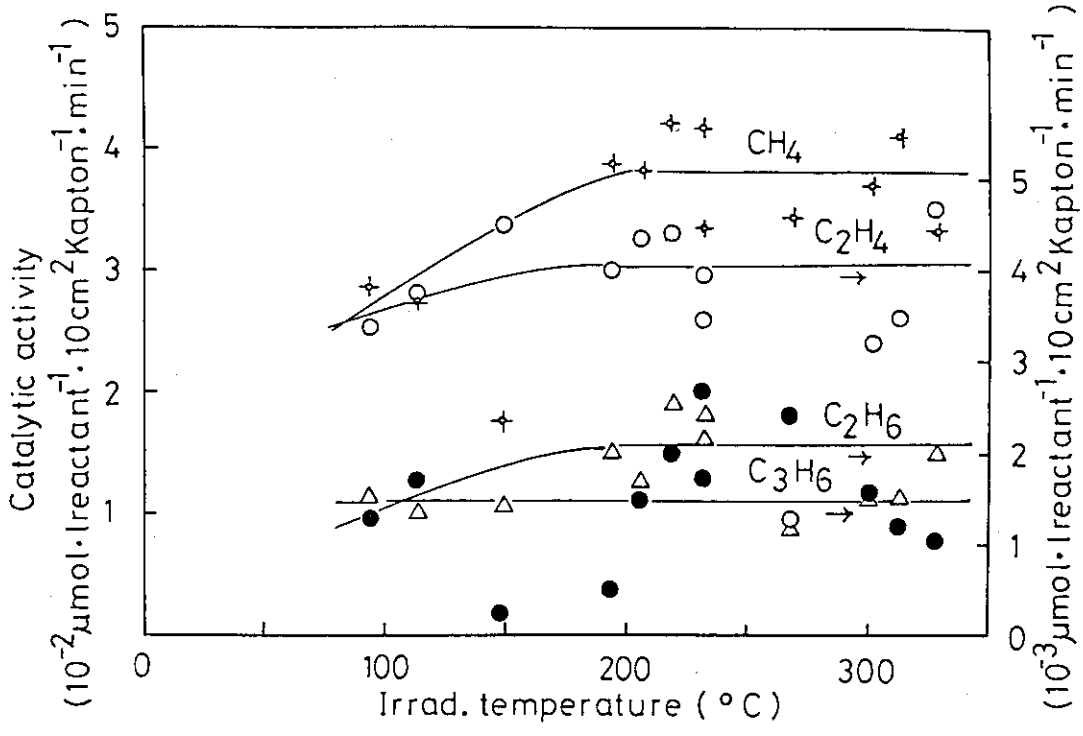

Fig. 3 Relation between catalytic activity and temperature at which the electron-beam doping was carried out.

rates shown in Fig. 3.

It is positively necessary to establish the quantitative method to obtain depth profile of iron which is implanted by the different experimental conditions for more detailed discussion of the results on activity reported in this report.

(S. Sugimoto, M. Hatada, and S. Nagai)

1) S. Sugimoto and M. Hatada, JAERI, 86-051, 16(1985).
2) T. Wada, Ohyobutsuri, 52, 239(1983).

5. Immobilization of Kr in Kapton Film

With the increase in nuclear power, many radioactive isotopes are generated by the fission of uranium-235, and remained in spent nuclear fuels. During fuel reprocessing procedures volatile gases are initially released from the fuel rods. Among these gases, krypton-85 has a sufficient long half-life, so it should be maintained safely for at least 100 years before being released in air.

Since krypton is a rare gas element and does not form stable compounds, it is stored at present in a high pressure cylinder. Because of the dangers of the storage at pressure as high as 14 MPa, alternative methods of reserving krypton are neccesary to be developed. Some of these methods are to reduce the pressure in the cylinder by the addition of charcoal, or zeolites.

Another alternative way is to immobilize it as minute gas bubbles in a metallic matrix by implantation using glow discharge. It is reported[1] that deposit of a sputtered-metal contains krypton atoms in concentrations up to about 14 atom%. Kr^+ implantation to organic polymer film(Kapton-H) is also reported,[2] to increase the electrical conductivity of the film due to the graphite formation, in which the amount of Kr atoms retained in the film is about one third of the nominal dose. The relationship between the graphitization of Kapton-H and the retention of the implanted Kr was investigated. The increase of the conductivity due to the graphitization was found to be fairly well proportional to the dosage.

Figure 1 shows the change of the X-ray surface diffraction pattern of Kapton-H films (thickness, 125 μm) by implantation of Kr at 40 and 200 keV. Though the diffraction curve is not changed by the implantation, the intensity decreases with the increase of accerelation voltage. The surface color of the

Kr-implanted sample becomes darker at a higher voltage indicating more intense graphitization.

Kr^+ implantation was also carried out on silicon wafer as the reference. The surface of the Kr-implanted sample seems to become rather porous with the increase of the Kr^+ acceleration voltage over 70 keV.

The quantitative analysils of the Kr-implanted surface of Kapton and silicon wafer is under investigation.

(Y. Nakase)

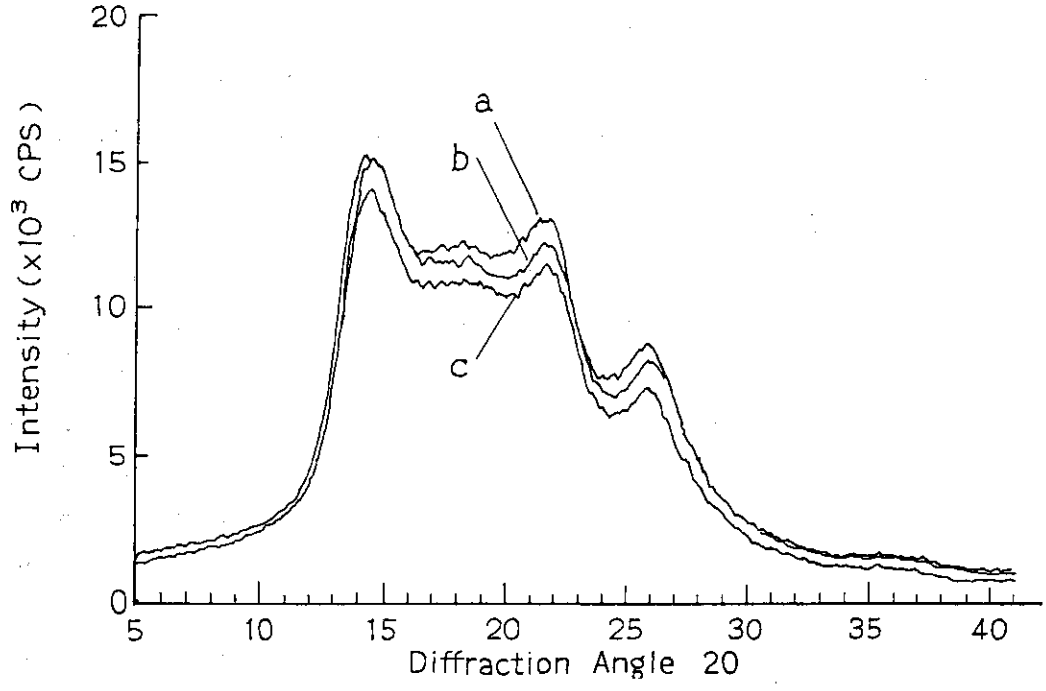

Fig.1 x-ray surface diffraction patterns of Kapton-H film (125 μm) Kr-implanted and the pristine (opposite side of the sample); (a) original film, (b) implanted with Kr^+ at 40 keV, and (c) at 200 keV.

1) G. L. Tinger, E. D. McClanahan, and M. A. Bayer, IAEA-SM-245/31, 1980.
2) T. Hioki, S. Noda, M. Sugiura, M. Kakeno, K. Yamada, and J. Kawamoto, Appl. Phys. Lett., 43(1) 30, 1983.

6. Thermally Stimulated Current of Irradiated Low Density Polyethylene

Thermoluminescence glow intensity and thermally stimulated current from irradiated low density polyethylene were measured as a function of temperature in an attempt to elucidate the mechanism of thermoluminescence in relation to the movement of charge carriers in the samples.

Low density polyethylene (Sumikathene G201F) was obtained from the Sumitomo Chemical Industries and was used after purification by precipitation from xylene solution. Some samples were used as obtained for reference purpose.

TSC measurements were carried out on the samples which were prepared by molding the polymer to a disk of 85 mm diameter and 0.1 mm thickness and then by pressing it between two sheets of aluminum foil which serve as electrodes. The thickness of aluminum foil electrode was thin as 17 μm so that depth dose curve of the incident electron beam was not affected by the electrode. Fig. 1 shows apparatus for TSC measurement. The sample was set in the irradiation chamber in that the two electrodes were short circuited and the irradiation was carried out in vacuum (10^{-4} Pa) at 77 K. After irradiation, DC voltage of 100 V was applied to the electrodes. After an initial transient period during which the current decreased to sufficiently low level, TSC was recorded as a function of time at a programmed rate of 10 K/min using a Keithley 617 electrometer. Since the TSC is given as a sum of current due to

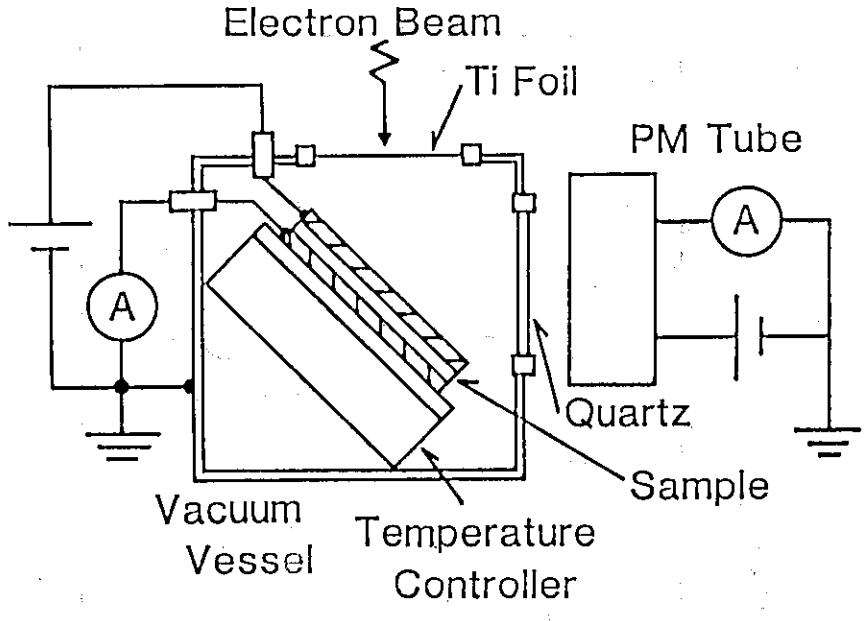

Fig. 1 Experimental apparatus for TSC and TL measurement.

thermal release of trapped carrier which was produced by the electron irradiation, I_{trap}, that due to arrangement of dipoles, I_{dipol}, and that due to conduction at thermal equilibrium, I_{therm}, according to eq. (1):

$$I_{TSC} = I_{trap} + I_{dipol} + I_{therm} \qquad (1)$$

I_{trap} was obtained as the difference between the current obtained on irradiated sample and that obtained on the sample without irradiation, cancelling the third and the fourth terms in eq.(1).

In Fig. 2, the I_{trap}-temperature curves were shown for the samples irradiated with doses from 20 kGy to 200 kGy. The peak appeared at 220 K and then the intensity increased above 240 K with increasing temperature.

The current increased with increasing dose, and the same

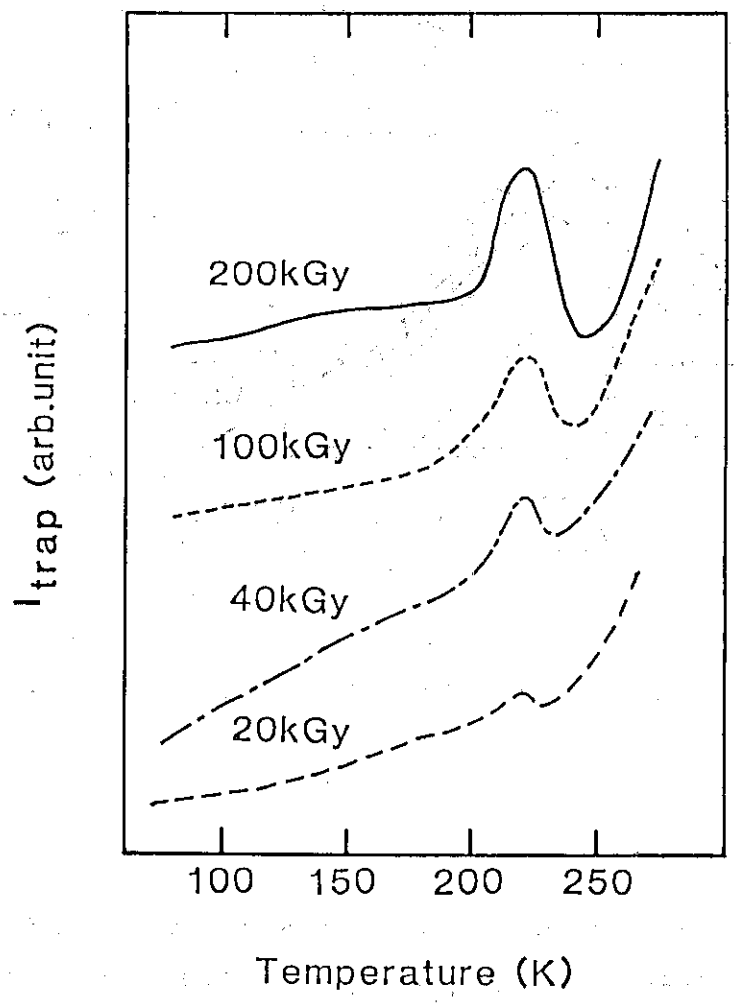

Fig. 2 Dose dependence of I_{trap}-temperature curves for low density polyethylene (Sumikathene G201F) at 10^{-4}Pa.

result was obtained for the samples without purification. Since the temperature at which the peak appeared (220 K) agrees with the temperature at which the molecular motion of polymer chain occurs (β-mechanical dispersion)[2], the increase in I_{trap} above 240 K seems to correspond to α-dispersion.[3] The current increase can be ascribed to thermal release of trapped carriers related to the molecular motion of the polymer chain.

TL and I_{trap}-temperature curves obtained for samples irradiated with 100 kGy were shown in Fig. 3, where both curves give maximum at 220 K indicating that TL appeared at this temperature is related with the thermal release of trapped carriers. Since I_{trap} showed no peak at 110 K, the TL peak at 110 K comes from some phenomenon which is not related to charge carrier. The fact that the increase of I_{trap} above 240 K did

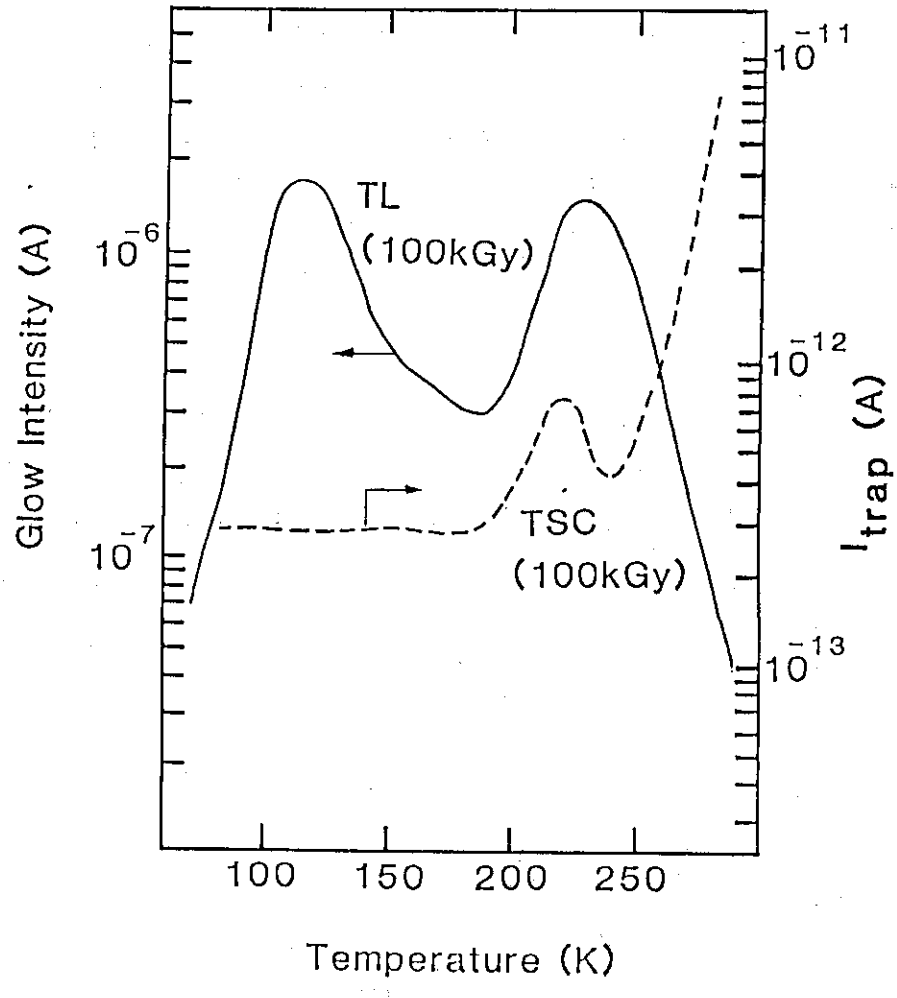

Fig. 3 Glow intensity and I_{trap} as a function of temperature for low density polyethylene (Sumikathene G201F) at 10^{-4}Pa.

not accompany the emission of light indicates that release of carrier above this temperature did not contribute to the emission of light.

Suppose small conductive particles (e.g. carbon) were present in the polyethylene sample, the released carrier would move through the conductive particles without exciting the insulating polyethylene medium. Thus, the following experiment was carried out in an attempt to estimate mean distance of carrier migration resulting in luminescence, and the result is shown in Fig. 4, where the intensity of thermoluminesence is given as a function of mean distance between carbon particles which is calculated from the amount of the carbon particles and mean diameter of the particles. The intensity decreased with increasing the amount of the particle above 0.3% indicating that the mean migration distance contributing optical emission is 80 - 130 μm.

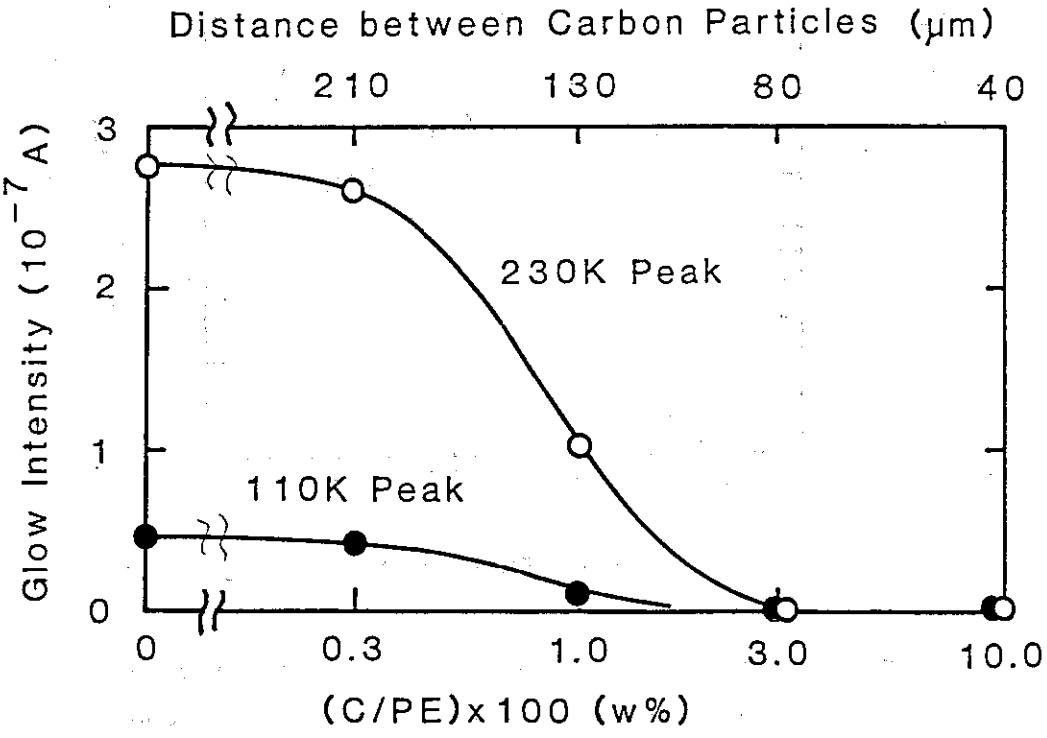

Fig. 4 Glow intensity as a function of carbon content.

TL spectra were measured for the peaks at 110 K and 230 K on the samples irradiated with 20, 40, 100 and 400 kGy. Both spectra at 110 K and 230 K measured on the samples irradiated with 20 and 40 kGy were similar in shape one another: peak appeared at 430 nm for 110 K peak and 350 nm for 230 K peak. The spectra obtained for the samples irradiated with higher doses (100 and 400 kGy) were different from those with the lower doses: both peaks at 110 K and at 230 K gave peak at 516 nm. The peak at 350 nm is assigned as one due to impurity whereas those at 431 nm and 516 nm may be assigned to CH(A-X) band and C_2(A-X) band, respectively, but further study is necessary for the elucidation of the above experimental results.

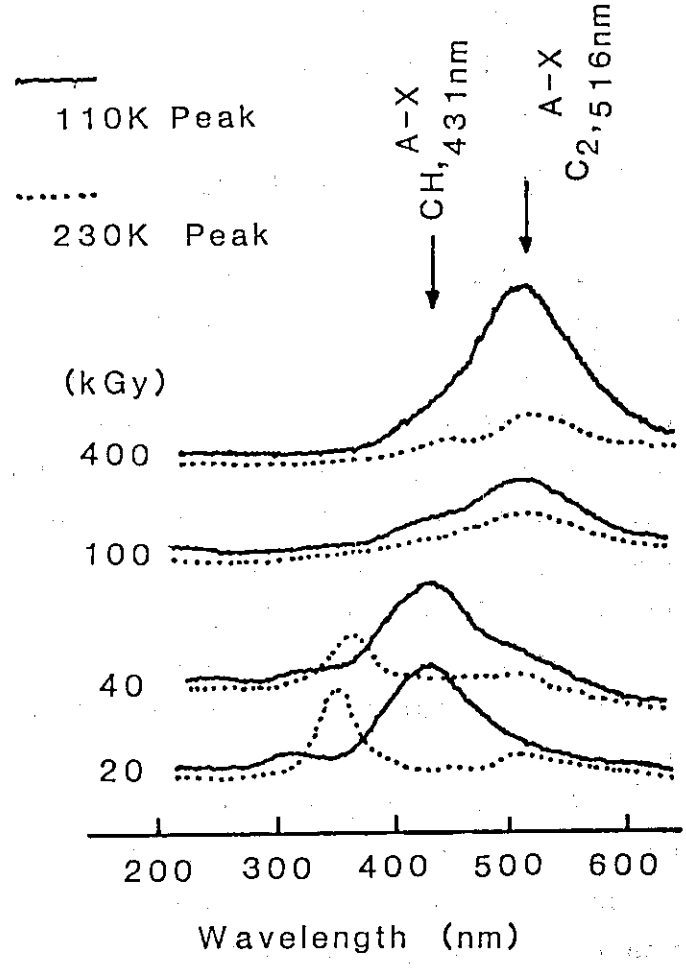

Fig. 5 Dose dependence of thermoluminescence spectra for low density polyethylene (Sumikathene G201F) at 10^{-4}Pa.

(K. Matsuda and Y. Tsuji)

1) K. Matsuda and Y. Tsuji, JAERI-M 86-051, P.21(1985).
2) Y. Wada, Physical Properties of Polymers, Baifukan,

Tokyo, 1971, p.381.
3) H. Watanabe and Y. Awakuni, IEEJ Trans. A, 106, 259(1986).

7. Dosimetry in the Glow Discharge Plasma Polymerization

In the last annual report[1] we described experimental results of the comparative studies on glow discharge polymerization and electron beam-induced polymerization in an attempt to obtain thin polymer films. It seems that whether the polymer was obtained in a form of powder or in a form of thin film depends on the energy absorbed in the system. However, the evaluating method of the absorbed energy is well established for the radiation chemistry of gases but not for the plasma chemistry in a sense that the absorbed energy scale is the same for both systems to allow quantitative comparative study.

This year experiments have been carried out in an attempt to evaluate the energy absorbed in the chemical reaction in the plasma using an N_2O dosimeter which is widely used in the gas phase radiation chemistry.

The plasma reactor used is the same as that used in the previous year, and the gas is excited by 13.55 MHz r.f. power. The composition of the gas in the reactor during discharge was determined by a quadrupole mass filter(NEVA), which is connected to the reactor through a leak (Fig. 1). The leak was designed so that the mass spectrum is obtained with the quick response to the change of the gas composition in the reactor which is shown in Fig. 2, where ion currents of N_2O^+(a), N_2^+(b) and O_2^+(c) change when RF discharge initiated and then reach the stationary value within one minute. Thus, the all mass spectra were taken at least one minute after reaction condition was changed.

A thermocouple gauge attached to the reactor monitors the gas pressure. Flows of nitrons oxide passes through 1.5 mm i.d. stainless tubing and a leak valve. A flow meter of float type monitors the flow rate. The reacted gas was pumped out by a mechanical pump (168 l/min.).

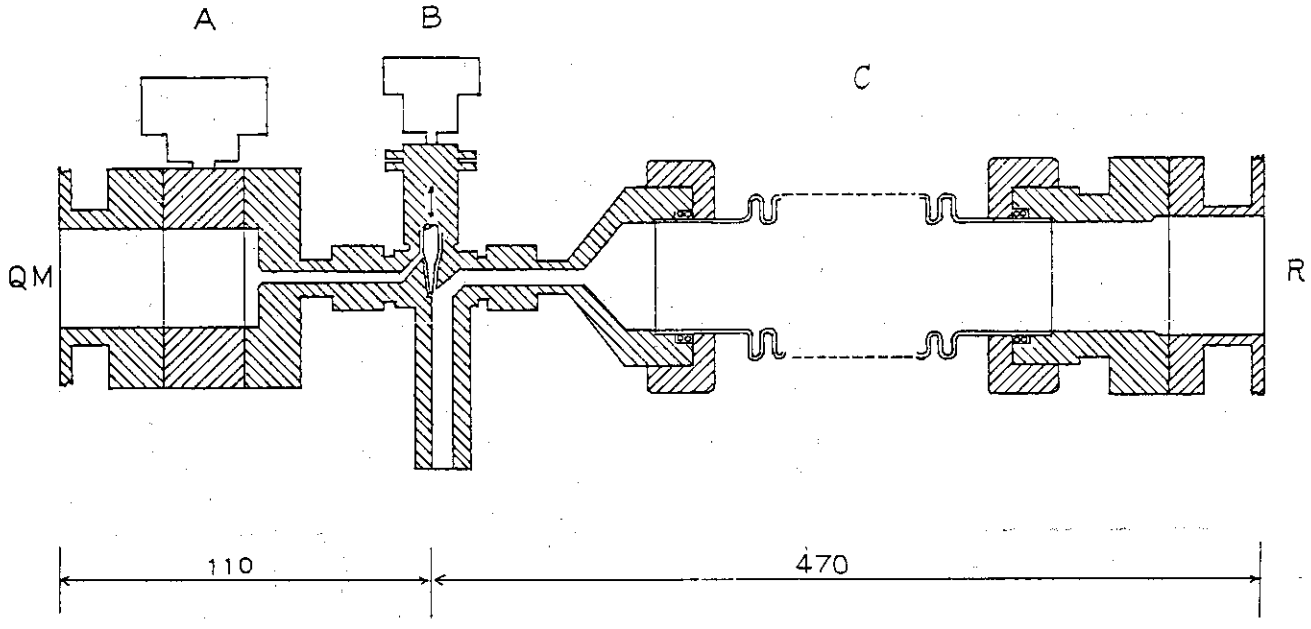

Fig. 1 Gas leak valve to introduce reactant gas Q-pole mass filter L(QM) with quick response. (A) Valve #304-24VFO, (B) fine metering valve #SS-6L, (C) flexible below connector #321-24-X-12, (D) ICF flange, and (R) flange to reactor.

Table 1 Mass spectra of the discharge reactor at different pressures and powers.

Flow rate (ml/min)	Pressure (Pa)	RF power (W)	Ion cuurrent (arbitrary unit) Mass number 18	28	30	32	40	44
0	<.01	0	4.2	1.7	0.0	0.8	0.0	0.8
1	10	0	5.1	12.5	14.7	1.3	0.1	36.3
1	10	1	5.2	22.2	5.4	4.8	0.4	10.5
		3	5.8	20.6	1.8	3.0	0.8	10.9
		8	6.3	31.0	1.0	3.9	0.2	5.9
		10	5.8	35.2	1.0	4.1	0.2	6.7
		20	6.8	39.3	0.9	2.8	0.3	7.0
		40	7.3	43.1	0.8	1.6	0.3	6.2
3	19	1	3.6	18.1	10.0	4.3	0.4	20.3
		3	3.4	28.2	6.0	7.8	0.6	11.4
		5	3.1	27.5	4.5	8.1	0.5	9.0
		10	3.5	27.9	2.3	6.5	0.0	7.5
		20	5.2	37.6	1.7	6.4	0.8	8.5
		40	7.2	45.3	1.0	4.0	1.3	8.6
5	25	1	2.7	13.5	9.6	3.2	0.3	21.7
		3	2.3	20.0	8.1	6.0	0.3	17.0
		5	2.8	28.5	7.0	9.5	0.6	13.1
		10	3.9	39.8	6.1	12.3	0.7	15.1
		20	5.3	41.5	4.4	10.9	0.9	10.1
		40	7.3	50.4	2.5	11.3	1.0	11.7
8	30	1	3.0	16.0	14.2	3.5	0.4	34.1
		3	2.8	26.8	14.1	7.4	0.2	30.0
		5	3.0	32.3	12.0	10.3	0.4	21.8
		10	3.1	41.7	11.1	14.0	0.4	15.7
		20	3.5	49.1	7.0	15.6	0.6	12.4
		40	5.7	60.3	6.1	16.7	0.7	13.5
15	38	1	2.7	22.3	22.1	3.0	0.2	67.4
		3	2.6	29.6	18.8	7.4	0.3	50.7
		5	3.1	35.5	19.1	10.4	0.2	37.0
		10	4.0	58.0	21.8	18.3	0.6	34.5
		20	4.1	58.1	14.2	20.1	0.4	24.5
		40	4.6	71.7	10.7	23.3	0.0	19.6
30	60	1	3.9	14.6	17.6	1.5	0.1	47.7
		3	3.8	17.0	17.2	3.2	0.5	42.3
		5	3.6	17.4	13.9	3.9	0.5	30.3
		10	2.7	21.7	13.1	6.0	0.6	26.8
		20	3.0	29.2	12.6	9.2	0.5	22.7
		40	4.1	47.0	13.9	15.2	0.6	22.3
50	90	1	4.2	23.3	30.0	1.6	1.0	80.7
		3	3.0	16.2	20.9	2.6	0.9	76.5
		5	3.0	19.7	20.2	4.0	0.3	50.0
		10	3.0	23.5	18.8	5.9	0.3	45.4
		20	3.1	32.0	19.0	9.2	0.5	38.0
		40	3.9	46.4	21.2	14.7	0.7	34.3
(Sensitivity)			1.30	1.00	1.00	1.00	0.83	0.72

Table 2 Cracking patterns.

m/e	Cracking patterns — Mass number			
	28	30	32	44
N_2	100.0	-	-	-
NO	-	100.0	2.4	-
O_2	2.0	-	100.0	-
N_2O	10.8	31.1	-	100.0

Table 1 lists the mass spectra of the gas eluted out from the reaction vessel obtained under different flow rates and discharge powers. The mole fraction of the component gas was calculated on the basis of the above data by solving a set of simultaneous equations using cracking patterns of the standard gases listed in Table 2 and the results are given in Table 3. The average residence time (sec) of the gas in the reaction vessel was calculated by

$$t = \frac{V \times P}{FR \times 1.01 \times 10^5 \times 60}$$

where FR is the flow rate (ml/min.), P, Pressure (Pa), and V, volume of the reaction vessel (ml). The reduced rate of reaction(R_r) at unit pressure in the vessel in μ mol$\cdot$sec$^{-1}\cdot$Pa^{-1} is calculated by

$$R_r = \frac{dn}{dt} = \frac{FR(1 - x_{N_2O})}{P} \times \frac{273 \times 10^6}{60 \times 22400 \times T}$$

where n is the number of N_2O molecule reacted, x_{N_2O}, mole fraction of N_2O in the reacted gas, and T, the room temperature (K).

The results of some typical calculations of R_r under different flow rates and RF powers are given in Table 4, and

Table 3 Mole fraction of the reactant and products in the discharge chamber during discharge at different experimental conditions.

Flow rate (ml/min)	Pressure (Pa)	RF power (W)	Mole fraction N_2	NO	O_2	N_2O
1	10	0	.038	.015	.010	.938
1	10	1	.487	.043	.108	.363
		3	.538	-.071	.072	.460
		8	.753	-.027	.083	.190
		10	.759	-.031	.078	.194
		20	.799	-.034	.044	.191
		40	.852	-.028	.017	.159
3	19	1	.260	.053	.079	.609
		3	.503	.039	.148	.310
		5	.543	.029	.167	.260
		10	.626	-.008	.145	.237
		20	.694	-.027	.114	.218
		40	.777	-.038	.060	.202
5	25	1	.168	.036	.061	.736
		3	.327	.040	.119	.514
		5	.459	.042	.168	.330
		10	.520	.007	.173	.299
		20	.612	.012	.165	.211
		40	.658	-.025	.150	.217
8	30	1	.108	.020	.048	.824
		3	.264	.039	.098	.599
		5	.374	.056	.140	.430
		10	.481	.070	.175	.274
		20	.572	.031	.190	.207
		40	.615	.012	.176	.196
15	38	1	.043	-.042	.023	.976
		3	.171	-.008	.073	.764
		5	.277	.055	.107	.561
		10	.397	.071	.145	.387
		20	.469	.046	.179	.306
		40	.557	.028	.192	.223
30	60	1	.019	-.012	.011	.982
		3	.076	.014	.036	.874
		5	.153	.043	.057	.748
		10	.235	.050	.090	.625
		20	.340	.062	.129	.469
		40	.446	.061	.161	.333
50	90	1	.016	-.012	.007	.989
		3	-.046	-.093	.019	1.120
		5	.074	.012	.041	.873
		10	.136	.017	.064	.783
		20	.246	.052	.098	.604
		40	.347	.077	.133	.444

Table 4 Reduced reaction rates obtained under different experimental conditions.

Flow rate (ml/min)	Pressure (Pa)	Residence time(min)	RF Power 1W		3W		10W		20W		40W	
			R	Rr	R	Rr	R	Rr	R	Rr	R	Rr
1	10	1.000	0.043	0.004	0.441	0.044	0.558	0.056	0.561	0.056	0.583	0.058
3	19	0.632	0.081	0.043	1.435	0.076	1.587	0.084	1.626	0.086	1.660	0.087
5	25	0.500	0.913	0.037	1.682	0.067	2.425	0.097	2.734	0.109	2.710	0.111
8	30	0.374	0.975	0.033	2.222	0.074	2.360	0.078	4.396	0.147	4.460	0.149
15	38	0.253	0.249	0.007	2.452	0.065	6.369	0.168	7.214	0.190	8.080	0.213
30	60	0.200	0.374	0.018	2.620	0.044	7.588	0.126	11.039	0.184	13.870	0.231
50	90	0.178	0.381	0.011	-	-	7.519	0.084	13.720	0.152	19.260	0.214

R:reaction rate(μmole$\cdot$s^{-1}); Rr:reduced rate(μmole$\cdot$s$^{-1}\cdot$Pa^{-1})

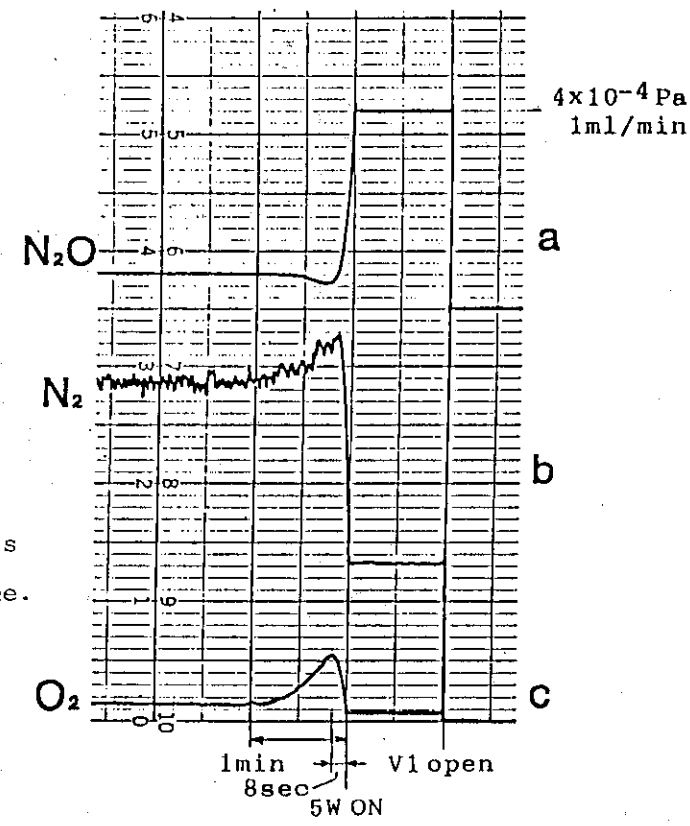

Fig. 2 Ion currents as a function time.

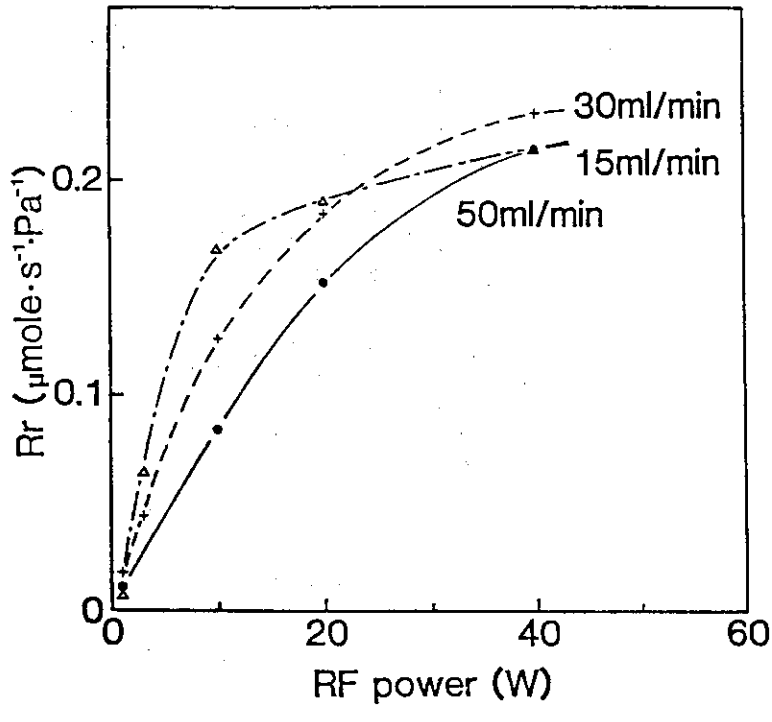

Fig. 3

Plot of reduced reaction rate as a function of RF power.

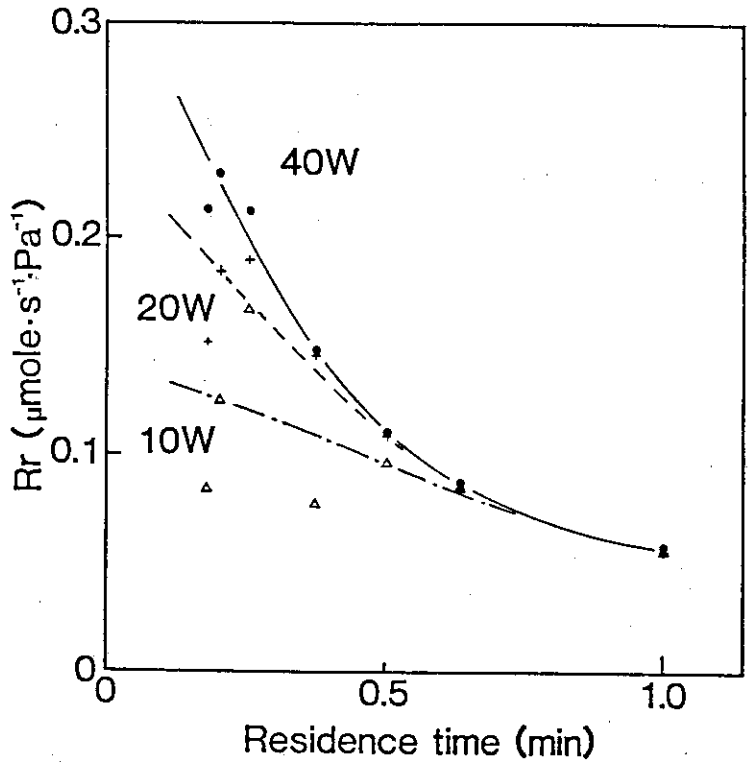

Fig. 4 Plot of reduced reaction rate as a function of residence time.

the plots of R_r as a function of residence time and RF power are shown in Figs. 2 and 3, respectively. Since the plots of data obtained at 40 W and at residence time of 29.6 min lie on smooth curves, these curves were used for further calculations. The best fit equations for the curve in Fig. 3 by regression analysis is:

$$R_r = 0.000595 + 0.00914\ W - 1.075 \times 10^{-4} W^2 \quad \text{---- (1)}$$

The rate at 40 W calculated as the linear extension of the slope at W = 0 is given by

$$\left(\frac{dR_r}{dW}\right)_{W=0} \times 40 = 0.009 \times 40 = 0.366 \quad (\mu\ \text{mole}\cdot s^{-1} Pa^{-1})$$

Similar analysis on the curve in Fig. 4 gives the following power series of residence time, t:

$$R_r = 0.3746-0.006537t+4.6283\times10^{-5}t^2-1.296\times10^{-7}t^3 \quad ----(2)$$

The R_r extrapolated to t = 0 gives 0.3746 μ sec·s^{-1}·Pa^{-1} which is close to that obtained from eq.(1)(0.366 μ sec·s^{-1}·Pa^{-1}).

The dose rate was calculated to be 2×10^{18} eV·s^{-1}·Pa^{-1} based on the G(-N_2O) value of 10.0 which is further converted to 1.8×10^7 rad·s^{-1} provided that the N_2O consumption found in this experiment is caused by the energy absorbed in the whole quantity of N_2O contained in the vessel (1.76×10^{-4} g·Pa^{-1}).

Since the dose rate at 20 W becomes 0.9×10^7 rad·s^{-1} or 0.9×10^5 Gy·s^{-1}, the dose rate obtained in the present research is about 5 times as low as the previously estimated value (4.3×10^5 Gy·s^{-1} at 20 W and 39.2 Pa).

(M. Hatada and T. Kijima)

1) M. Hatada, T. Kijima, and N. Kawakami, JAERI-M, 86-051, 29(1985).

8. Electron Beam Curing of Liquid Epoxy Oligomer

Epoxy oligomer containing onium salt can be cured by electron beam irradiation. Bisphenol A-diglycidyl ether (Epikote 828, M_N 324) and bis 4-diphenylsulfonio) phenyl sulfide-bis-hexafluorophosphate,[1] BDS(PF_6) were used as liquid oligomer and initiator, respectively. Epoxy oligomer containing the initiator(5×10^{-2} mol/kg, based on oligomer weight) was dissolved in THF and cast to a viscous liquid film on a slide glass plate. The plates were put in a draft and then in a vacuum oven at 30°C to remove THF. The oligomer films (11 mg/cm^2) were irradiated in air with electron beams of 1.5 MeV from a Van de Graaff accelerator. The irradiated films were subjected to extraction with acetone and gel contents were gravimetrically determined. A gel-dose curve at the dose rate

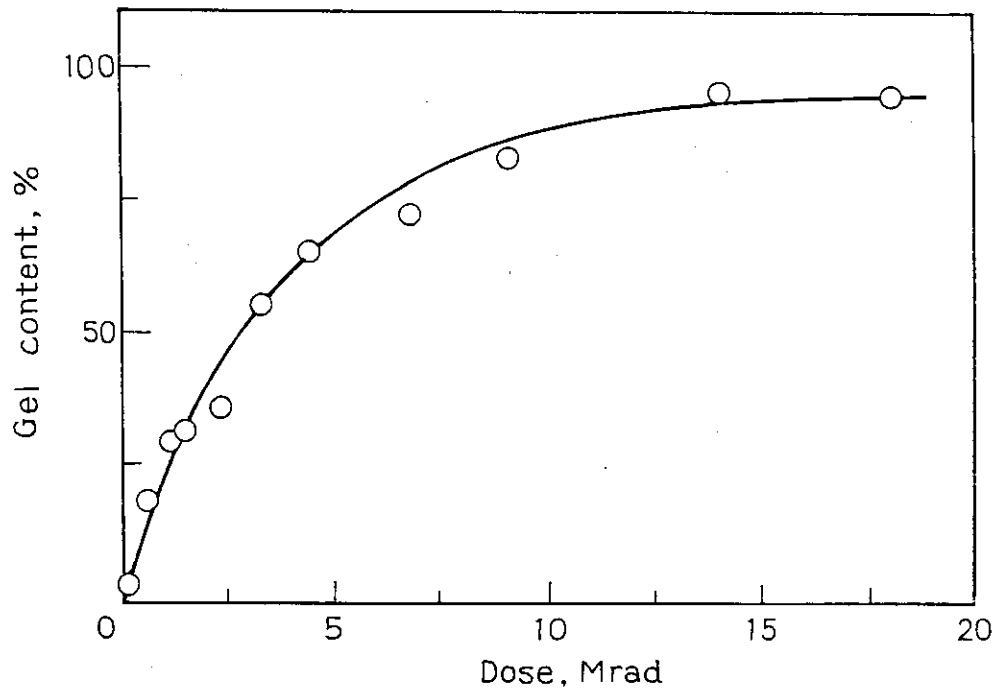

Fig. 1 Gel content in irradiated epoxy oligomer as a a function of 1.5 MeV electron beams at 0.075 Mrad/s. BDS(PF_6) 5.0 x 10^{-2}Mol/kg.

of 0.075 Mrad/s is given in Fig. 1. Gel content increases with increasing irradiation dose, reaching a levelling-off value of 95% at a dose of 13.5 Mrad. In absence of disulfonium salt epoxy oligomers do not polymerize on exposure up to 30 Mard of electron beam irradiation.

Infrared studies were carried out on epoxy oligomers to know the change of structure with irradiation. Thin film epoxy oligomers on KBr were prepared from THF solution. Infrared spectra were recorded from 4000 to 600 cm^{-1} on a Hitachi 270-30 IR spectrometer. The change in IR spectra with electron beam irradiation is shown in Fig. 2. On irradiation absorption of the epoxide group at 916 cm^{-1} increases as a result of opening and polymerization. Concurrently, increase in hydroxyl and ether bands in region of 3500 cm^{-1} and at 1108 cm^{-1} are observed. Phenyl band at 830 cm^{-1} remains constant regardless

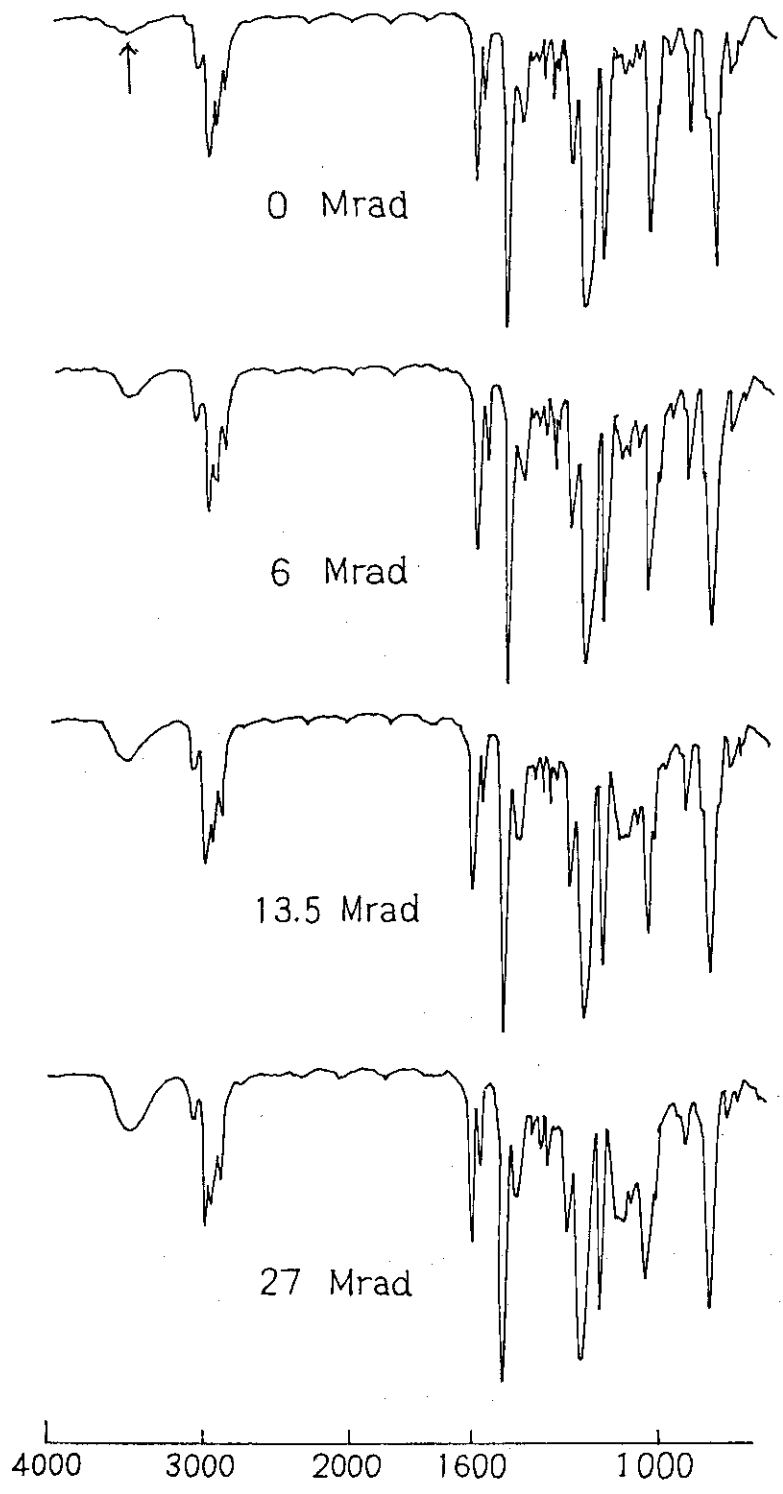

Fig. 2 Change in IR spectra of epoxy oligomer with electron beam irradiation. BDS(PF_6) 5.3 x 10^{-2}mol/kg.

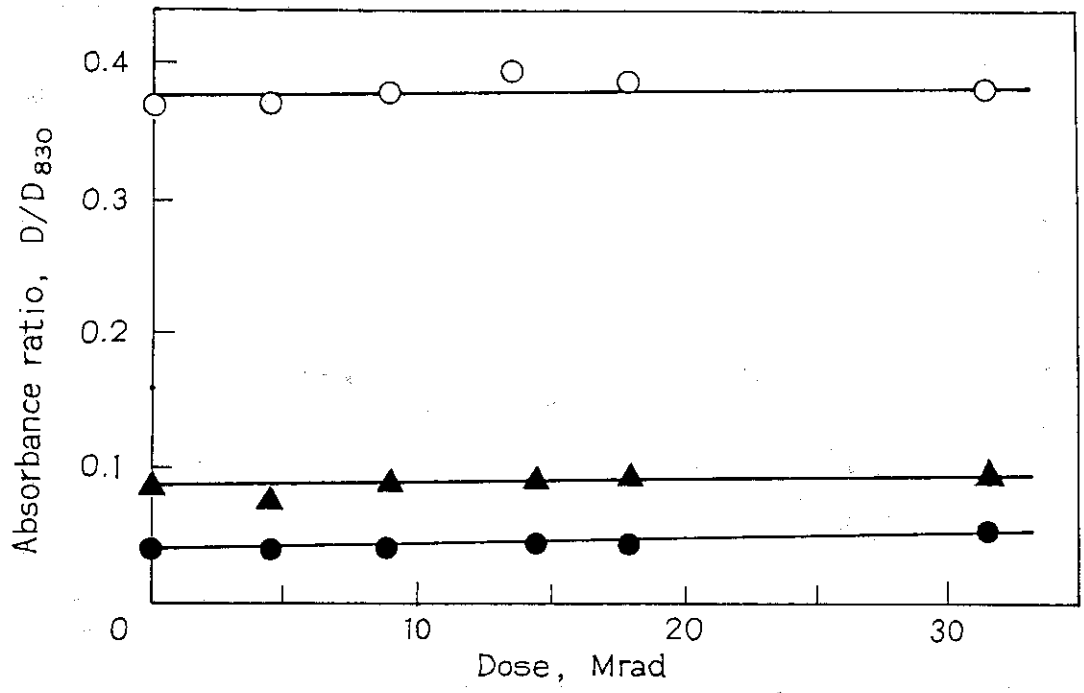

Fig. 3 IR absorbance of epoxide, 916 cm^{-1}(○), hydroxyl, 3500 cm^{-1}(●), and ether, 1108 cm^{-1}(△) in irradiation epoxy oligomer as a function of 1.5 MeV electron beams at 0.075 Mrad/s. Irradiations were carried out in absence of disulfonium salt.

of epoxide reaction. The band is used as an internal standard band. Without disulfonium salt no change in intensities of above three bands was observed up to 30 Mard as shown in Fig. 3. Absorption intensities of epoxide, hydroxyl and ether bands are given as a function of dose in Fig. 4. Intensity of epoxide band decreased monotonously, whereas those of hydroxyl and ether bands increased with irradiation dose up to 40 Mrad. Gel formation data revealed that gel content reached the levelling-off value at 13.5 Mrad and did not increase by further irradiation (Fig. 1). On the other hand infrared data indicate that epoxide group content still remains 60% of its initial quantitiy at 13.5 Mrad. Further irradiation brought about additional disappearance of epoxide to give a remaining

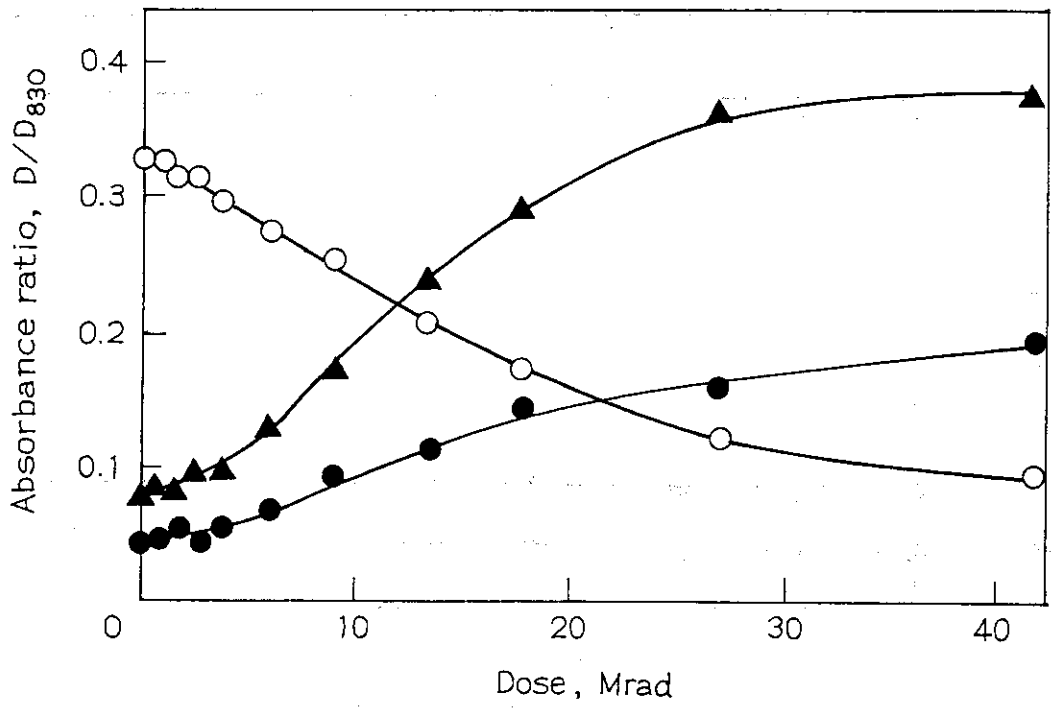

Fig. 4 Change in functional group content in epoxy oligomer with 1.5 MeV electron beams at 0.075 Mrad/s. BDS(PF_6) 5.3 X 10^{-2}mol/kg. symbols are the same as in Fig. 4.

value of 35% after irradiation of 40 Mrad. This finding shows that additional cross-linking reaction proceeds via epoxide opening after the gel content reaches the final value. This additional increase in cross-linking density was comfirmed by a dynamic visco-elastic studies.[2)]

The post-cure effect is known in ultra-violet irradiation of epoxide-sulfonium salt system.[3)] The present electron-initiated epoxide polymerization also shows substantial post-cure effect. The evidence of post-polymerization of epoxide after irradiation of electron beams has discontinued is obtained by observing change in the epoxide absorption band at 916 cm^{-1}. Decay curves of epoxide absorbances after three diffrent doses, 1.1 Mrad, 3.75 Mrad and 7.5 Mrad are shown in

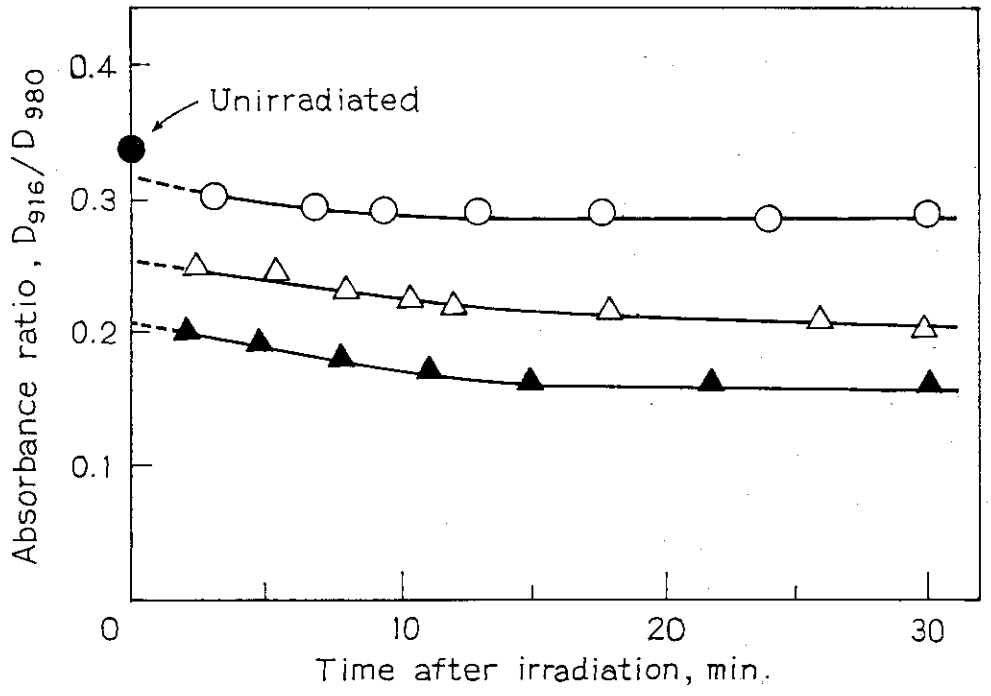

Fig. 5 Decay of epoxide absorption, 916 cm^{-1} after irradiation.
dose (○)1.1 Mrad, (△)3.75 Mrad, (▲)7.5 Mrad.

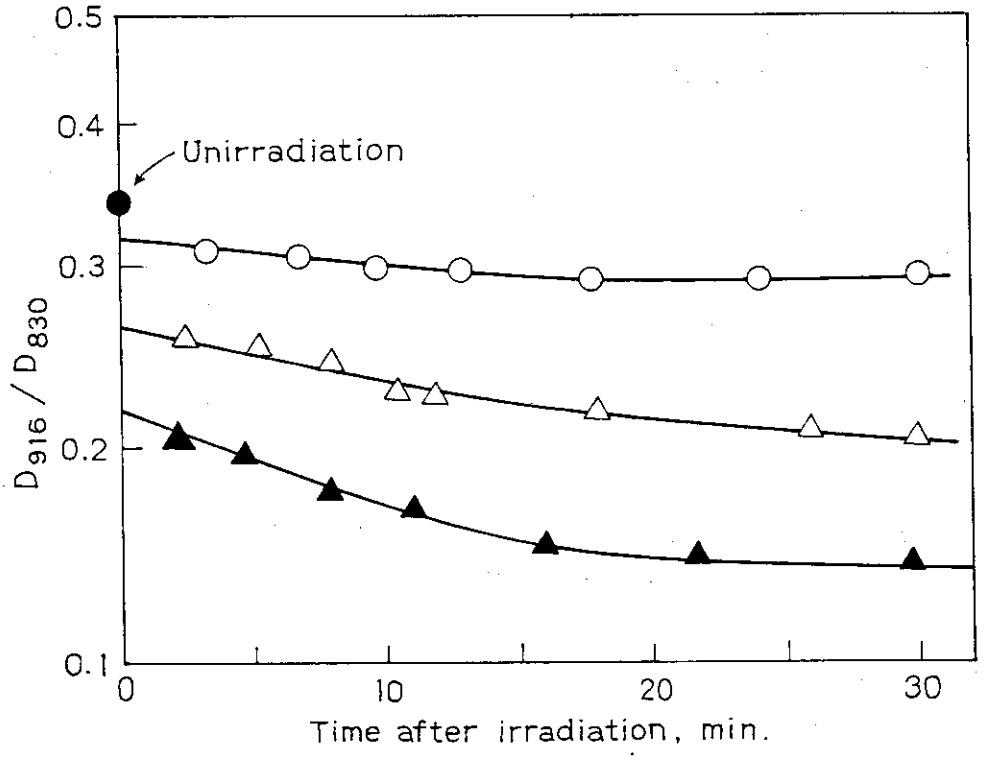

Fig. 6 Semi-log plots for decay of epoxide absorption, 916 cm^{-1} after irradiation.
Dose: (○)1.1 Mrad, (△)3.75 Mrad, (▲)7.5 Mrad.

Fig. 5. The first-order decay plots of epoxide absorbances are given in Fig. 6. Each decay curve can be represented by the two straight lines of different slopes. Rate constants of first-order decay, K in initial stage of standing time is proportional to irradiation dose, which is seen in Fig. 7. This means that the rate of formation of initiating species is proportional to the irradiation dose.

(T. Okada, T. Asano, J. Takezaki, and M. Hatada)

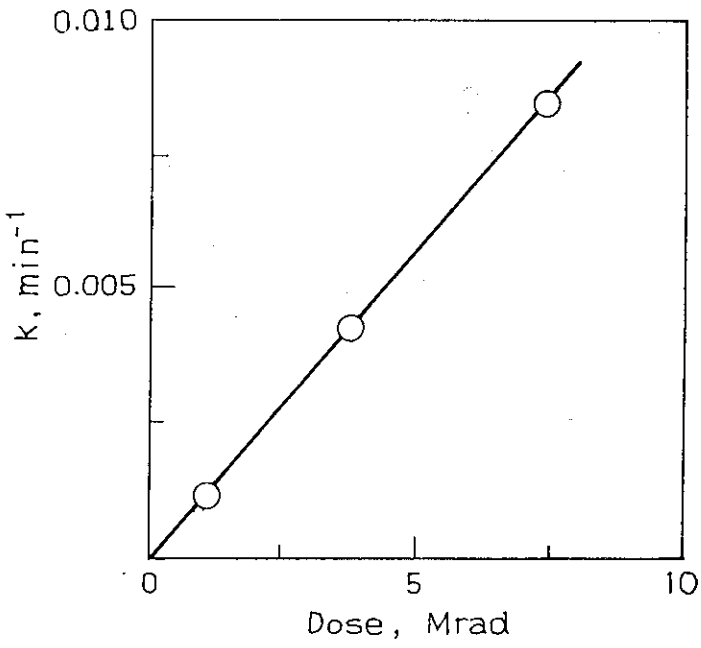

Fig. 7 Relationship between appearent rate constant of first-order decay and irradiation dose.

1) W. R. Watt, H. T. Hoffman, Jr., H. Pobiner, L. J. Schkolnick, and L. S. Yang, J. Polym. Sci., Polym. Chem. Ed., 22, 1789(1984).
2) T. Okada and T. Asano, Unpublished results.
3) W. R. Watt, "UV Curing, Science and Technology, Vol.II", S.P. Pappas, Ed., Technology Marketing Corp., 1985, P.225.

9. The Surface Structure of Polyethylene Film Grafted with Acrylic Acid with or without the Presence of Mohr's Salt

From the viewpoint of the regulation of the surface structure of graft copolymers it is important to investigate the positions and distributions of grafted components which

depend on the grafting conditions and processes.

For this purpose we selected a grafting system consisting of acrylic acid(AA) as a monomer, high density polyethylene(PE) as a trunk polymer, and Mohr's salt as an inhibitor to polymerization. Grafting was carried out in the AA aqeous solution with or without added Mohr's salt by preirradiation method. The positions and distributions of grafted poly(acrylic acid)(PAA) in the PE film are studied by optical microscopy, scanning electron microscopy(SEM), electron probe microanalysis(EPM), ATR-IR spectroscopy, and X-ray photoelectron spectroscopy(ESCA). Optical microscopic and EPM observations show that the grafting initiates at the film surface and the thickness of graft layer increases with increasing total graft percent in both cases with and without Mohr's salt. The grafted PAA distributes homogeneously throughout the graft layer, which means a sharp boundary between grafted and ungrafted regions. From the ATR-IR spectroscopic measurements it is clarified that in the case of grafting without salt the surface layer of the grafted film consists of only PAA and in the case with Mohr's salt it consists of both PE and PAA. The latter case suggests that the grafting is supressed outside the film owing to this inhibitor.

SEM photographs give us direct surface structures of the film. The starting PE film shows the typical shishikabab or row-nucleated structure on the surface; overgrowth lamellae are seen to be alligned normally to the machine direction. In the case of the 1.2% grafted film without Mohr's salt small grobules less than 1 μm in diameter are scattered on the surface. These grobules increase in both number and size with increasing the degree of grafting until they fuse together to form larger blocks and finally cover the surface structure of the initial PE film.

When the grafting is carried out in the system with Mohr's

salt, no globules are observed on the surface of the graft film and the lamellar structure still remains even if the degree of grafting is more than 10%. It is also supported from the result of ESCA that grafted PAA exists in the outermost surface layer about 40 Å thick.

Fig. 1 illustrates the schematic diagrams for the morphological structure of AA grafted PE film at the initial stage of grafting, which are drawn on the basis of the above observations by SEM and ESCA. Fig. 1a shows the microstructure

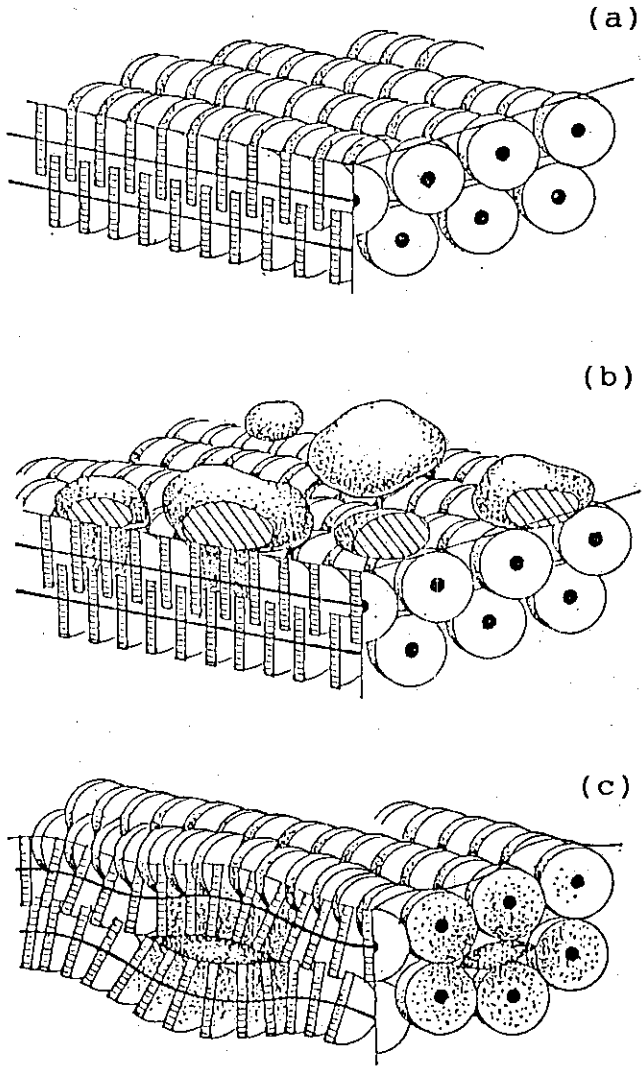

Fig. 1
Schematic drawing of acrylic acid grafted polyethylene film; (a)starting PE film, (b)grafted PE film prepared without Mohr's salt, (c)grafted PE film prepared with Mohr's salt.

of the surface and cross-section of the starting PE film in which the row-nucleated structure with piles of lamellae is drawn. Fig. 1b represents the structure of grafted film prepared without Mohr's salt. The radicals which migrated from the crystalline regions to the lamellar surfaces initiate grafting in the interlamellar regions, and the grafting proceeds rapidly outside the film to form globules of PAA since the diffusion rate of AA monomer outside the film is much higher than that inside the film. Fig. 1c is the case without added Mohr's salt, in which the grafting is also initiated in the interlamellar regions and the grown PAA penetrates among shishikababs to form lumps. These lumps bulge the film surface above them.

The distribution of PAA in the cross-section of AA-grafted PE film prepared by preirradiation method is also illustrated schematically in Fig. 2. The grafting starts at the film surface of PE since high density PE is not swollen in the AA aqueous solution and radicals to initiate the grafting are distributed in the PE film. In the grafting system without

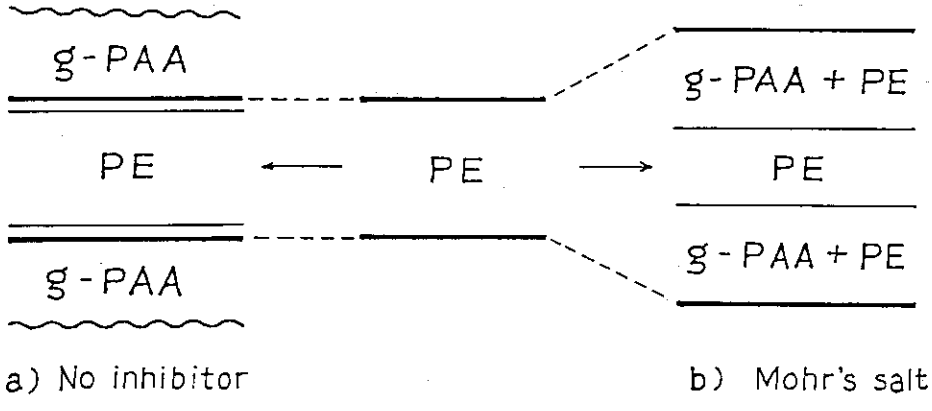

Fig. 2 Cross-sectional view of acrylic acid graft polyethylene film prepared without (a) or with Mohr's salt (b).

added salt (Fig. 2a) graft polymerization hardly proceeds inside the film because the diffusion rate of AA monomer into PE film is extremely slow compared with that in the solution. The grafting consequently proceeds outside the film at a high grafting rate to form the PAA surface layer, the thickness of which increases with increasing degree of grafting. On the other hand, in the grafting system with added Mohrs's salt (Fig. 2b), the graft polymerization proceeds inside the film since the growth of graft chains is prohibited outside the film because of the inhibitor existing in the solution. As a result, the graft layer consisting of PAA and PE is formed inside the film.

Experimental results described in this report indicate that the texture of the graft film can be controlled by selecting appropriate conditions of grafting.

(K. Kaji)

10. Reduction of Crystalline Units of Nylon 66 Films by Electron Beam-Irradiation studied by Melting Point Measurement-II

Study has been carried out this year on the depression of melting temperature by electron irradiation for nylon 66 film of low crystallinity and that after heat-treatment to increase its crystallinity at different degrees. The purpose of the present study is to establish the relation between the crystal structure of the film and the change of the amount of crystalline units and also between the film structure and the change of the length of crystallites, both changes being induced by electron irradiation.

Nylon 66 film of low crystallinity(40 μm thick) used in this study was supplied from Toray Co. Endothermic peak of this film by DSC was observed at 531 K. Heat-treatment for

annealing the film was carried out in vacuum at 508 K for desired time of period between 8 and 81 hrs. Electron beam irradiation was carried out using a Van de Graaff accelerator in nitrogen atmosphere at 343 K, 1.5 MV and 50 μA. The dose rate determined by CTA film dosimeter at this irradiation condition was 1.24 kGy/s. DSC measurement was carried out for 2 mg of sample in nitrogen atmosphere at a programmed rate of 15 K/min. The sensitivity was 0.010 J/s.

The degrees of crystallinity of the film as received were 26% as evaluated from absorbance of amorphous band at 1145 cm^{-1} and 29% as evaluated from the heat of fusion. Those of the film annealed at 508 K for 24 hrs were 41% and 46%, from IR method and DSC measurement, respectively.

X-Ray diffraction of the original film shows two diffuse reflection peaks corresponding to spacing of 3.98 and 4.23 Å. The spacings changed with annealing time as shown in Fig. 1, and after 30 min heat-treatment, the diffuse peaks became sharper and the spacings reached constant values of 3.694 and 4.361 Å which are characteristic of the α-form crystal.

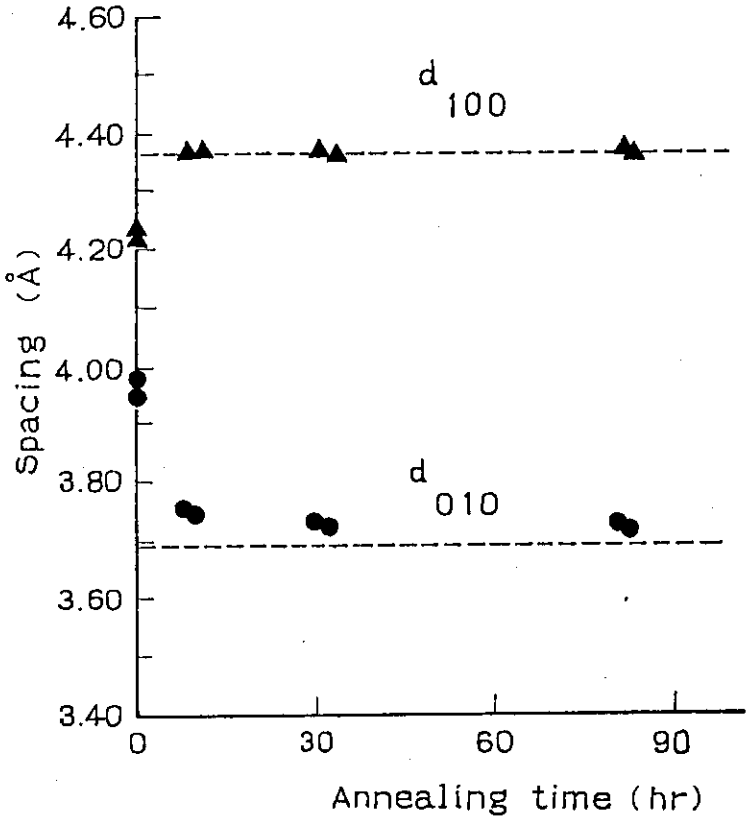

Fig. 1 Changes of spacing with annealing time at 508 K for nylon 66 films.

The absorption bands appeared at 1329 and 1224 cm^{-1} in the IR spectrum of the heat-treated film, which have been assigned as the deformation on vibrations of CH_2 group adjacent to amide group as the indication of the existence of a folded-chain structure of the film.[1] The band at 690 cm^{-1} which is assigned as the out-of-plane deformation of N-H bond (known as the amide V band) increased its intensity by the heat-treatment, indicating that distortion of N-C bond between two adjacent main chains decreased by the heat-treatment.[2]

Consideration of the X-ray diffractions and IR spectra led us conclusion that in the original film, the polymer chain in an intermediate state of order in which polymer chain rotates around its chain axis in the form of hexagonal-closest packing, whereas in the annealed film the film is composed of crystallites termed as α-form, in which polymer chain takes a folded-chain structure.

Fig. 2 shows the depression of melting point of un-annealed and annealed films as a function of dose at 343 K. The melting point of the un-annealed film decreased linearly at 0.020 K/kGy with dose to 511 K by 1000 kGy irradiation. The melting point of annealed film decreased similarly with dose at low dose below 100 kGy, and then decreased linearly at 0.0034 K/kGy to 525 K by the irradiation of the same dose.

Gel fraction of irradiated film both un-annealed and annealed increased with increasing dose as shown in Fig. 3, but the dose giving the same gel fraction differs significantly each other: the dose resulting in gel fraction of 0.6 was 330 kGy for the former, while it was 500 kGy for the latter.

The mole fraction of crystalline units, X and the length of crystallite, ℓ (cm) can be calculated from the melting point of the film using Flory's melting equation and Thomson-Gibbs' equation, respectively.[3] In Fig. 4, the mole fraction of crystalline units and the length of crystallite thus obtained

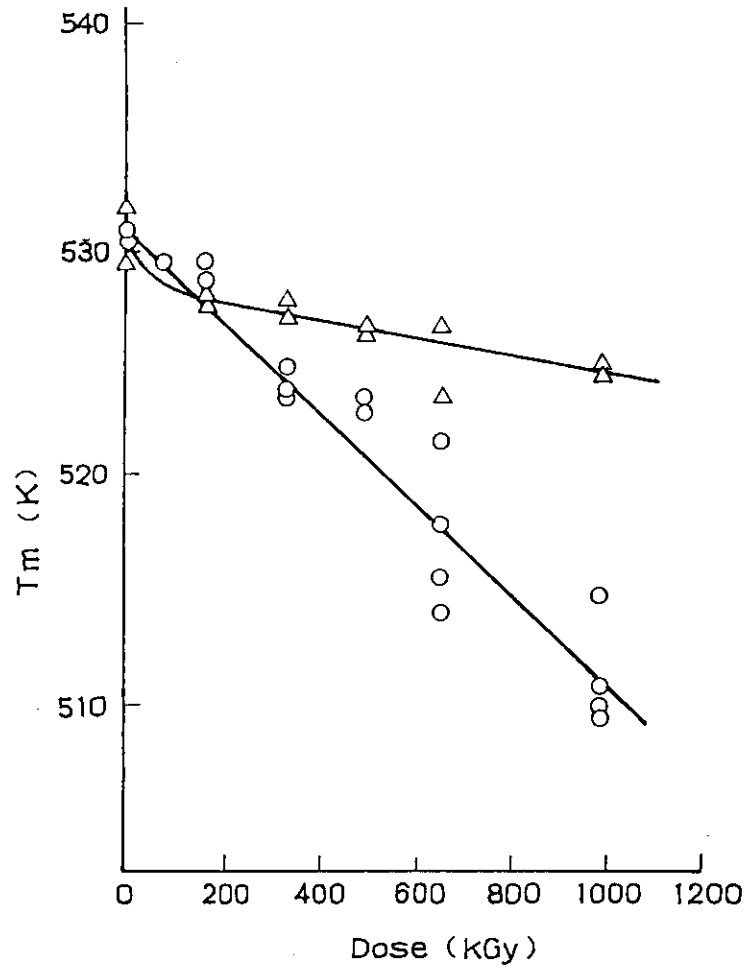

Fig. 2
Dependence of Tm on dose for un-annealed (○) and annealed (△) nylon 66 films. Annealing: 508 K, 24 hrs in vacuum
Irradiation: 343 k in N_2

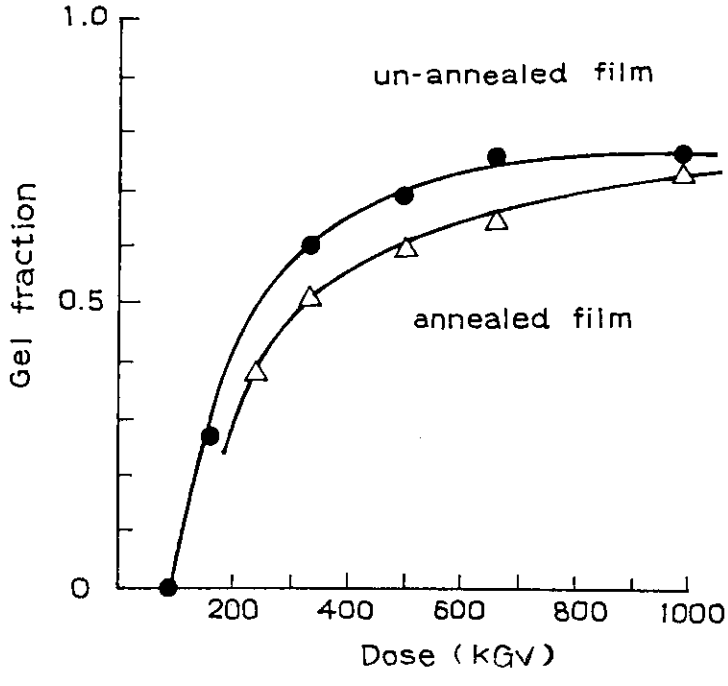

Fig. 3
Gel fraction vs. dose for irradiated un-annealed (●) and annealed (△) nylon 66 films.
Annealing: 508 K, 30 hrs in vaccum Irradiation: 343 Kin N_2

are plotted as a function of dose. By 1000 kGy irradiation the mole fraction of crystalline unit and the length of crystallite decreased to the values which are 70% of the original ones for un-annealed film, whereas by the irradiation of the same dose of the annealed film these values do not decreased below 90% of the original values.

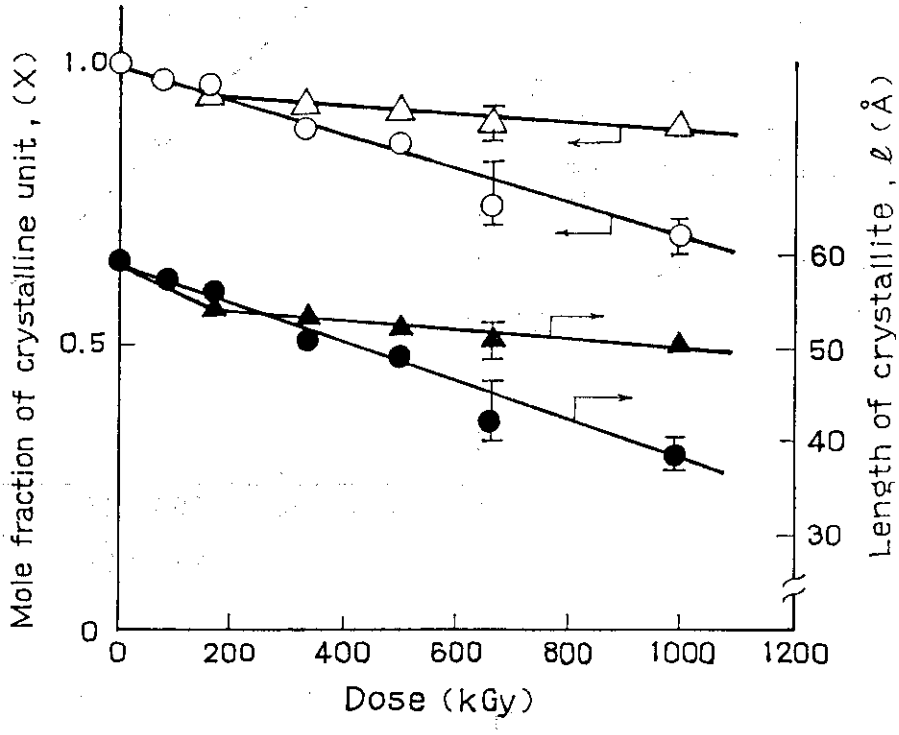

Fig. 4 Dependences of mole fraction of crystalline unit and length of crystallite on dose for un-annealed (○,●) and annealed(△,▲) nylon 66 films.
Annealing: 508 K, 24 hrs in vaccum
Irradiation: 343 K in N_2

The result that the increase of gel fraction is not accompanied by the decrease of the mole fraction of the crystalline units in the annealed film indicates that the cross-linking occurred mainly in amorphous part. It was

concluded that the high mobility of the polymer chain due to distortion around chain axis in the hexagonal-closest packing in the crystalline part of un-annuealed film makes it possible to cross-link even in crystalline part from the experimental results that the amount of crystallite decreased with increasing gel fraction by irradiation.

(M. Nishii)

1) J. L. Koenig and M. C. Agbortwalla, J. Macromol. Sci.-Phys., B2, 391(1968).
2) A. Miyake, J. Polym. Sci., 44, 223(1960).
3) B. Wunderlich, "Macromolecular Physics," Vol. 3. Crystal Melting, Academic Press, 1980.

III. LIST OF PUBLICATIONS

[1] Published Papers

1. K. Matsuda, "Thermoluminescence Glow Curves of Irradiated PMMA and Low Density Polyethylene", JAERI-M 85-044.

2. T. Oshiyama, S. Nagai, K. Ozawa, and F. Takeuchi, "Data Compilation for Particle Impact Desorption II", JAERI-M 85-100.

3. K. Kaji, "Radiation Grafting of Acrylonitrile onto Polyester Fiber as the Reinforing Fiber for Poly(vinyl chloride)", JAERI-M 85-175.

4. S. Sugimoto, M. Nishii, and T. Sugiura, "Radiation-Induced Chemical Reactions of Carbon Monoxide and Hydrogen Mixture 2. Effects of Reactant Pressure and Temperature on the Yields of Oxygen Containing Products", Radiation and Physics, Vol. 26, 715(1985).

5 S. Sugimoto, M. Nishii, and T. Sugiura, "Radiation-Induced Chemical Reactions of Carbon Monoxide and Hydrogen Mixture 3. Solid Materials Produced under Irradiation", Radiation Physics and Chemistry, Vol. 27, 147(1986).

6. S. Sugimoto, M. Nishii, and T. Sugiura, "Radiation-Induced Chemical Reaction of Carbon Monoxide and Hydrogen Mixture 4. On the Water Produced by the Addition of Small Amounts of Ammonia", Radiation Physics and Chemistry, Vol. 27, 153(1986).

7. K. Matsuda, S. Tanaka, S. Takaore, and C. Inagaki, "Molecular Size and Characteristics of Anion Sensitive Site of Microsomal Anion-Sensitive Mg^{2+} -ATPase in Rat Brain", Biochimca et Biophysica Acta.

[2] Oral Presentations

1. S. Nagai, "Electron and Ar^{+} Ion Beam Induced Adsorption and Desorption Processes of Gases at Alumina Surface", The 9th Symposium on Ion Sources and Ion-Assisted Technology, (Tokyo), Jun. 4, 1985.

2. S. Sugimoto and M. Hatada, "Catalytic Activity of Kapton Film Implanted with Fe by Electron-Beam Assisted Recoil Implantation", 51st Annual Meeting of The Chemical Society of Japan (Kanazawa), Oct. 1-4, 1985.

3. K. Matsuda, H. Izumi, and Y. Tsuzi, "Thermoluminescence Spectra of Low Density Polyethylene", Physical Society of Japan (Chiba), Oct. 2, 1985.

4. M. Nishii, and A. Taguchi, "Dependence of Depression of Melting Point on Crystalline Structure in Nylon 66 Films Irradiated by Electron Beam", The Joint Meeting of Kyushu, Chugoku and Shikoku Branches of The Chemical Society of Japan (Ohita), Nov. 4, 1985.

5. S. Nagai, "Ion Impact Desorption of Gases Adsorbed on Al_2O_3 and TiC", The 28th Discussion Meeting of Radiation Chemistry (Sapporo) Nov. 6, 1985.

IV. EXTERNAL RELATIONS

A training program for scientists and engineers in industries and government organizations was held in the laboratory as one of the courses offered by the Radio-isotope school, JAERI in Tokyo. This one week program starting Oct. 21 included lectures and laboratory experiments concerned with the radiation chemistry of polymers from its basic subjects to recent application in industries. We welcomed 13 trainees this year.

Some studies in this laboratory were conducted under the cooperative agreements with Prof. Y. Tsuji of Kinki University and with Prof. H. Saito of Naruto College of Education, and four coperative studies were initiated this year. They are those with Prof. Kosai of Osaka Electrocommunication University, Prof. Y. Ikada of Kyoto University, Prof. K. Hatada of Osaka University, Prof. T. Okada of Ohita University, and Prof. T. Oshiyama of Kyoto Sangyo University.

Three joint research programms were initiated this year with industrial companies: they are Matsushita Electric Industries, Ltd., Shyowa Kobunshi Co., and Seiren Co. A sponsored investigation was made under the contract with the Mitsubishi Electric Corporation.

On Oct. 4th, Professor Su Jia Zhen of Changshung Institue of Applied Chemistry, Chinese Academy of Sciences of People's Republic of China visited the laboratory to discuss about recent progress on applied and pure radiation chemistry of polymers in both institutions.

Dr. Kanako Kaji was a visiting lecturer at Chemical Institute of Chinese Academy of Sciences in Beijin from Aug. 1 through Aug. 19.

V. LIST OF SCIENTISTS

(March 31, 1986)

[1] Staff Members

Motoyoshi HATADA	Dr., physical chemist, Director
Seizo OKAMURA	Professor emeritus, Kyoto University, Advisor
Yoshiaki NAKASE	Dr., polymer chemist
Siro NAGAI	Dr., physical chemist
Shun'ichi SUGIMOTO	Physical chemist
Koji MATSUDA	Radiation physicist
Jun'ichi TAKEZAKI	Physical chemist
Masanobu NISHII	Dr., polymer chemist
Kanako KAJI	Dr., polymer chemist
Yuichi SHIMIZU	physical chemist